Punjab University Journal of Mathematics (2026), 58(03), 386- 418
https://doi.org/10.52280/pujm.2026.58(03)05

Demonstration of Soliton Wave Structures in a Higher-Dimensional Nonlinear Physical Model: Dynamic Insights into Sensitivity, Bifurcation, and Chaos

Received
12 June, 2026

Revised
27 July, 2026

Accepted
07 August, 2026

Published Online
17 August, 2026

*Muhammad Iqbal, Muhammad Aziz ur Rehman
Department of Mathematics,
University of Management and Technology, Lahore, Pakistan

Zaheer Hussain Shah
Department of Physics,
University of Management and Technology, Lahore, Pakistan

Abstract. This article presents a comprehensive analytical and dynamical investigation of the (4+1)-dimensional variable-coefficient generalized Kadomtsev Petviashvili equation (vc-gKP). Exact analytical solutions are constructed using the modified Khater method, constructing a diverse class of localized and propagating wave structures that capture the intrinsic nonlinear characteristics of the governing model. To further examine the system, an extensive dynamical analysis is carried out using phase-plane trajectories, temporal evolution, Poincaré maps, bifurcation analysis, and Lyapunov exponents, allowing the identification of distinct dynamical states and their transitions. The obtained results reveal a variety of complex nonlinear behaviors, including periodic oscillations, quasi-periodic motion, chaotic dynamics, and multistable responses associated with both softening and hardening nonlinear effects. To further verify these behaviors, power spectral analysis, recurrence plots, return maps, and fractal dimension calculations are incorporated, providing complementary information regarding the spectral distribution, geometric organization, and complexity of the resulting attractors. The corresponding numerical illustrations clearly demonstrate the evolution of the system from regular to chaotic regimes together with the coexistence of multiple stable attractors under different parameter conditions. Overall, the proposed analytical and computational methodology establishes an effective framework for exploring nonlinear wave phenomena in higher-dimensional evolution equations and contributes to a deeper theoretical understanding of models arising in fluid mechanics, plasma physics, nonlinear optics, and related branches of mathematical physics.

**Corresponding Author* :iqbalakhtar167@gmail.com

AMS (MOS) Subject Classification Codes: 35S29; 40S70; 25U09
Key Words: Dynamical behavior; Chaotic behavior; Bifurcation diagram; Sensitivity analysis; Multistabilty analysis.

1. INTRODUCTION

The mathematical modeling of nonlinear phenomena largely relies on nonlinear partial differential equations (NLPDEs), which serve as a powerful framework for analyzing complex dynamical systems. Because of their effectiveness in capturing nonlinear interactions, these equations have attracted considerable attention and have been widely used in diverse fields, such as fluid dynamics, telecommunications, medicine, biological sciences, solid-state physics, neuroscience, life sciences, geochemistry, hydrology, and mechanics [1]. It is also widely applied in chemical reaction kinetics [2], plasma physics [36], and complex dynamical system theory [22]. Because of these characteristics, in particular the ability of the NLPDEs for modeling highly nonlinear systems, they have become a key ingredient for building some physical, biological, and chemical behaviors. These equations, which possess soliton waves that propagate at a constant speed while maintaining their structure and amplitude, hold a special place as a significant breakthrough in applied mathematics and mathematical physics [26]. In recent times, studies of higher-order fractional differential equation. and nonlinear pseudo-Hermitian models resulted in an impressive development in finding their analytical exact or approximate solutions by various techniques such as the variational iteration method [11], integral transform methods [28], the simplified Hirota method [35], $e^{-\psi(\zeta)}$-expansion approach[7], Laplace transform method [15], the B$\ddot{a}$cklund transformation method [21], and Lie symmetry analysis [14]. These techniques remain useful for developing models to explore quantitative and qualitative dynamics of nonlinear evolution equations (NLEEs).

The history of soliton theory can be traced back to the pioneering observations of John Scott Russell [23]. In 1834, he made an experiment on water wave motions in the Union Canal of Great Britain and found an interesting phenomenon: a single wave-like hump traveling a long distance without changing its shape. He called it Great Translation Wave. Although it was an extraordinary observation, at first it was not accepted by the mathematical world. In particular, George Biddell Airy expressed skepticism and published in his Tides and Waves of 1845, showing that the velocity of long waves depends on both the height and the depth. However, Russell insists that a single wave is capable of going long distances without distorting itself and degenerating with notable dispersion [12]. Moreover, the studies of Lord Rayleigh and Joseph Boussinesq in the 1870s provide a mathematical foundation for this behavior [37]. Their theoretical developments lead to an interesting nonlinear partial differential equation proposed by Diederik Korteweg and Gustav de Vries in 1895, which is now well-known as the Korteweg-de Vries (KdV) equation [18], and the KdV equation serves as a principal tool for describing solitary wave dynamics in shallow-water regions. A significant step towards understanding nonlinear wave dynamics came in 1955 when Fermi, Pasta, and Ulam conducted a computer simulation on a one-dimensional nonlinear lattice to observe the phenomenon of energy flow [9]. Their purpose was to find out the process of energy exchange between vibrational modes. They originally predicted the energy would gradually be uniformly distributed between various modes, but instead, the system returned close to its initial state, with an uneven distribution between modes. This recurrent phenomenon is now known as the Fermi-Pasta-Ulam (FPU) problem.

In 1965, Zabusky and Martin Kruskal [40] revisited the FPU problem to gain a deeper understanding of the observed recurrence phenomenon. They encountered the unusual interaction of solitary waves when simulating the nonlinear lattice KdV equation numerically. During the collision of two solitary waves, both solitons emerged from the interaction with exactly the same shape, velocity, and amplitude. The surprising stability of these waves has led to a comparison with elementary particles (protons, electrons, and photons) and to the coinage of the name soliton. The theory, however, had no mathematical framework to solve the initial value problem for the nonlinear integrable partial differential equations. In 1967, the initial value problem for a broad class of integrable nonlinear evolution equation was systematized by Gardner, Kruskal, Miura, and Greene (GKMG) by their development of the IST. The mathematical theory, later termed the Lax pair, for the integrability of nonlinear evolution equations was then developed by Lax [19]. An even wider class of integrable nonlinear partial differential equations was then formulated, and the IST was used for the nonlinear Schrödinger equation to obtain exact solutions consisting of solitons by Zakharov and Shabat [30], thus expanding greatly the domain and range of solitons to encompass different types such as topological and non-topological [8]. In non-linear classical field theory, topological solitons are stable finite-energy localized smooth configurations with features resembling those of magnetic monopoles, whereas the other widely cited family is envelope solitons, which are wave packets localized in space, propagating in a dispersive non-linear medium [17]. Depending on the profile of the wave packet, envelope solitons are further classified as either bright or dark depending on the shape of the wave packet. Bright solitons refer to the fact that the wave has a spike localized in space riding over a constant wave field, whereas dark solitons consist of a localized dip with a constant wave field. Within the NLSE description, bright solitons exist for anomalous dispersion, whereas dark solitons exist for normal dispersion [13].

The primary objective of this work is to investigate the proposed nonlinear model from both analytical and dynamical viewpoints. The exact wave solution is obtained by using the modified Khater method (MKM). This method is a new kind of analytical technique for constructing closed-form exact solutions to NLEEs. The MKM method, developed by Khater et al.[6], is also known as the modified extended auxiliary equation method. This technique has an expansive range of applicability, such as being simple in implementation, economically cost-saving, and readily constructing different branches of exact solutions through not needing to perform laborious symbol manipulation. The derivation of MKM is presented based on the auxiliary equation method to construct explicit solutions of nonlinear PDES with integer as well as fractional order. A novel method that generates so many solution families of various solitary wave structures for a mathematical model [32]. Due to all the above properties, it was successfully explored for the study of solutions of the nonlinear Schroedinger, fractional STO, Bogoyavlenskii system, and telecommunication fractional equations [5].

To investigate the qualitative dynamics of the proposed vc-gKP equation, bifurcation analysis is performed by examining the influence of the governing parameters on the system behavior [10]. Transformation of the governing equation using proper variables becomes equivalent to an equivalent dynamical system; equilibrium solutions for this system will be obtained. Using a Jacobian matrix, we may determine the local stability of these solutions. This analysis enables the identification of different categories of equilibrium points, such as saddle, center, and cusp points, while also revealing the geometric structure of the phase space and the transition mechanisms responsible for changes in the system dynamics. Consequently, bifurcation analysis provides valuable insight into the long-term evolution of plasma wave interactions and their sensitivity to parameter variations. Moreover, dynamical analysis showed that the system has chaotic behavior in some range of parameter. These parameters showed very strong dependence to the variation of parameter, a slight change in parameters leads to much more difference in dynamics of the system which reflects that the model is nonlinear and behavior of the system varies non-linearly. The result proved that the nature of the system is highly nonlinear, hence parameter variations have to be controlled while studying the models. Thus by observing the variation of parameter, structure of the bifurcation and the chaos analysis we found the nature of the system. Therefore, bifurcation and Chaos are fundamental nonlinear dynamics phenomena found in various domains such as economics, ecology, telecommunications, engineering and many others. It is useful in order to predict, if a periodically perturbed system exhibits the chaotic response or not. Study of these transitions also gives a deeper insight in to how the system responds for various conditions of parameter variations. Several researchers have recently explored the bifurcation characteristics of nonlinear dynamical systems from different perspectives.Recent studies have extensively employed bifurcation theory to explore the dynamics of nonlinear systems. Recent advances have highlighted the significant role of bifurcation analysis in revealing the complex dynamics of nonlinear wave equations. Jhangeer et al.[16] investigated bifurcation-driven pattern formation in nonlinear traveling-wave systems. Li et al.[20] analyzed bifurcation phenomena in higher-order nonlinear Schrödinger equations. Similarly, Tang et al.[33] explored the bifurcation characteristics of a nonlinear Boussinesq equation with power-law nonlinearity, while Mezamo et al.[25] examined the bifurcation behavior of a subcritical complex Ginzburg–Landau equation in the presence of both local and global time-delay effects.

Inspired by these contributions, the present study focuses on the vc-gKP equation, which serves as an important mathematical model for describing multidimensional nonlinear wave propagation in dispersive media. The classical Kadomtsev–Petviashvili (KP) equation was proposed by Boris Kadomtsev and Vladimir Petviashvili in 1970 to describe the propagation of weakly nonlinear ion-acoustic waves in plasma under the influence of weak transverse disturbances. Owing to its ability to capture multidimensional nonlinear wave phenomena, the KP equation has become one of the most extensively studied models in nonlinear wave theory. It has been successfully employed to describe both internal and surface water waves, as reported by Ablowitz and Segur, and has also found important applications in nonlinear optics through the work of Pelinovsky, Stepanyants, and Kivshar. Due to the fact that the KP equation is able to describe the interactions among multi-dimensional nonlinear waves, for decades the KP equation has continuously paid close attention to a large quantity of branches of mathematical physics. Except for the initial KP equation, the KP-type models have successfully been utilized to investigate the wave phenomena in plasma, fluid, and other dispersive media, being particularly effective in the study of nonlinear, long-wavelength, shallow wave equations in 2D plasma. Researchers try many types of generalized KP models to address more abundant physical backgrounds. In this work, our attention is directed toward the (4+1)-dimensional vc-gKP equation proposed in [27], which serves as the mathematical model investigated throughout this study.

$$\begin{aligned}\mathcal{F}_{xt} + A\left(\mathcal{F}\mathcal{F}_x\right)_x + B\mathcal{F}_{xxxx} + C_1\mathcal{F}_{xx} + C_2\mathcal{F}_{xy} + C_3\mathcal{F}_{xz} + C_4\mathcal{F}_{xs}\\ + C_5\mathcal{F}_{yy} + C_6\mathcal{F}_{zz} + C_7\mathcal{F}_{ss} = 0.\end{aligned} \tag{1. 1}$$

In Eq. (1. 1), the dependent variable $\mathcal{F}(x, y, z, s, t)$ denotes the wave amplitude, while x, y, z, s, and t correspond to the spatial and temporal independent variables. The parameters A and B account for the nonlinear and dispersive characteristics of the governing equation, respectively. The time-varying perturbation effects are represented by the coefficient functions $C_i(t)$ for $1 \leq i \leq 4$, whereas the coefficients $C_i(t)$ with $5 \leq i \leq 7$ describe the variable wave velocities along the x, y, z, and s-directions. The KP and its nonlinear generalizations are widely applied to the research of nonlinear wave models, so the equations have already been analyzed by several analytical methods. Some published studies have reported exact analytical solutions for a variety of nonlinear evolution equations. Wang found exact solutions of the Kadomtsev–Petviashvili–Benjamin–Bona–Mahony equation [38], the Camassa–Holm–Kadomtsev–Petviashvili equation [39]. In addition, exact wave solutions expressed in terms of Jacobi elliptic functions were derived using the Jacobi elliptic function method [34]. Ali et al. [3] applied the ϕ_6-expansion method to construct exact solutions of the coupled Higgs equation. Similarly, the Hirota bilinear method was employed to obtain soliton solutions of the Bogoyavlenskii–Kadomtsev–Petviashvili equation [4]. Although these studies successfully derived exact analytical solutions, their primary emphasis was on solution construction rather than on the investigation of the associated nonlinear dynamical behavior.

The remainder of this paper is organized as follows. Section 2 presents the formulation and implementation of the MKM. Section 3 represents the graphical behavior of exact solutions. Section 4 is devoted to the derivation of comprehensive dynamical investigation, including phase portraits, time-series analysis, Lyapunov exponents, Poincaré maps, bifurcation diagrams, multistability, power spectrum analysis, fractal dimension, return maps, recurrence plots, and sensitivity analysis. A qualitative comparison of the present results with existing studies on the KP equation is provided in Section 4. Section 5 shows the comparsion of current and previous study. Finally, the principal findings and concluding remarks are presented in Section 6.

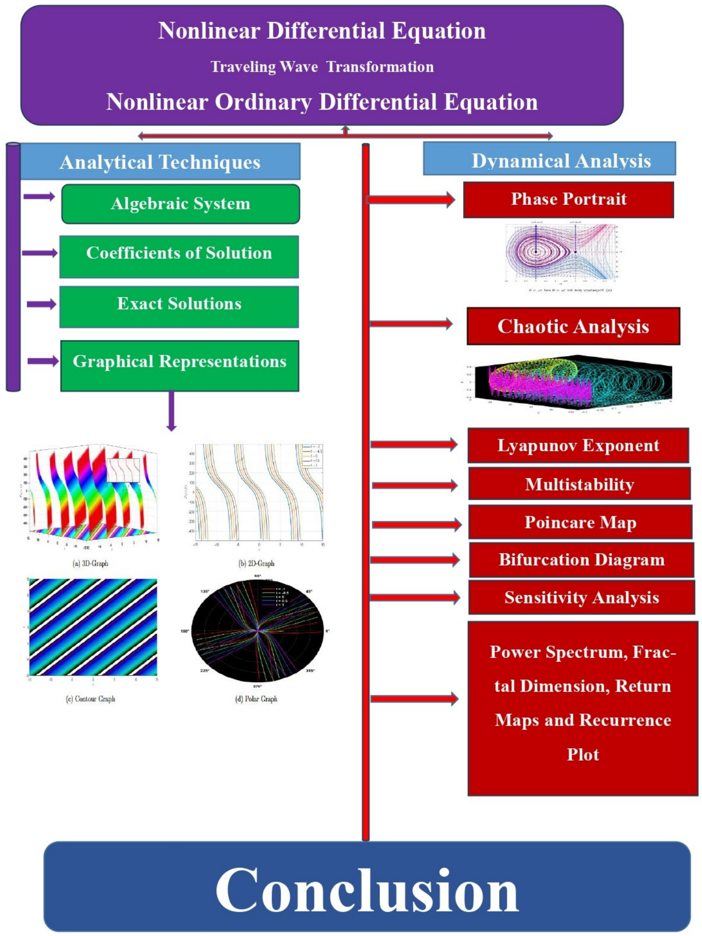

FIGURE 1. Graphical Paper Layout.

2. EXECUTION OF TRAVELING WAVE

The general procedure for transforming the governing nonlinear partial differential equation into its corresponding nonlinear ordinary differential equation is summarized below.
Step (1): Consider the general form of a nonlinear partial differential equation (NLPDE),

$$K(\mathcal{F}, \mathcal{F}_x, \mathcal{F}_y, \mathcal{F}_z, \mathcal{F}_s, \mathcal{F}_t, \mathcal{F}_{xx}, \mathcal{F}_{xy}, \mathcal{F}_{yy}, \mathcal{F}_{xt}, \mathcal{F}_{yt}, \ldots) = 0, \tag{2. 2}$$

where $\mathcal{F} = \mathcal{F}(x, y, z, s, t)$ denotes the dependent variable, and K represents a nonlinear polynomial operator involving $\mathcal{F}$ together with its partial derivatives of different orders.
Step (2): Introduce the traveling wave transformation

$$\mathcal{F}(x, y, z, s, t) = \mathcal{G}(\Psi), \qquad \Psi = kx + ly + mz + ns - \omega t, \tag{2. 3}$$

where k, l, m, and n are the wave numbers associated with the spatial coordinates, while ω denotes the wave speed.
Step (3): Substituting the transformation given in Eq. (2. 3) into Eq. (2. 2) transforms the original NLPDE into a nonlinear ordinary differential equation (NODE) with respect to the traveling wave variable Ψ, given by

$$\begin{aligned}&\left(C_1k^2+C_2kl+C_3km+C_4kn+C_5l^2+C_6m^2+C_7n^2\right)\mathcal{G}''-k\omega\mathcal{G}''\\&\quad+Ak^2\left((\mathcal{G}')^2+\mathcal{G}\mathcal{G}''\right)+Bk^4\mathcal{G}''''=0.\end{aligned} \tag{2. 4}$$

This can be written in a simplified form as

$$-k\omega\mathcal{G}^{''}+Ak^2\left(\mathcal{G}^{'2}+\mathcal{G}\mathcal{G}^{''}\right)+Bk^4\mathcal{G}^{''''}+P\mathcal{G}^{''}=0, \tag{2. 5}$$

where

$$P=C_1k^2+C_2kl+C_3km+C_4kn+C_5l^2+C_6m^2+C_7n^2.$$

Integrating Eq. (2. 5) twice yields

$$Bk^4\mathcal{G}^{''}+(P-k\omega)\mathcal{G}+\frac{Ak^2}{2}\mathcal{G}^2=0. \tag{2. 6}$$

2.1. **Implementation of the Modified Khater Method.** To derive exact solitary-wave solutions of the proposed nonlinear evolution equation, the MKM is employed. The principal steps of the method are outlined as follows.
Step 1: Consider the general n-th order nonlinear partial differential equation (NLPDE)

$$H(\mathcal{F}_{xx},\mathcal{F}_{xy},\mathcal{F}_{yy},\mathcal{F}_{xt},\mathcal{F}_{yt},\ldots)=0, \tag{2. 7}$$

where $\mathcal{F}=\mathcal{F}(x,y,z,s,t)$ denotes the dependent variable, and H is a nonlinear polynomial operator involving $\mathcal{F}$ and its partial derivatives.
Step 2: Introduce the traveling-wave transformation

$$\mathcal{F}(x,y,z,s,t)=\mathcal{G}(\Psi),\qquad \Psi=kx+ly+mz+ns-\omega t, \tag{2. 8}$$

where k, l, m, and n are the wave numbers corresponding to the spatial coordinates, and ω represents the wave speed. Substituting Eq. (2. 8) into Eq. (2. 7) transforms the governing NLPDE into the NODE

$$H\left(\mathcal{G},\mathcal{G}',\mathcal{G}'',\mathcal{G}''',\ldots\right)=0. \tag{2. 9}$$

Step 3: Assume that the solution of Eq. (2. 9) can be represented by the finite polynomial expansion

$$\mathcal{G}(\Psi)=\sum_{j=0}^{N}\Lambda_j\Pi^j(\Psi), \tag{2. 10}$$

where $\Pi(\Psi)$ is an auxiliary function and Λ_j $(0\leq j\leq N)$ are constants to be determined. The value of N is obtained by balancing the highest-order derivative term with the dominant nonlinear term in Eq. (2. 9). For the present equation, the balancing procedure gives $(N=2)$. Therefore, Eq. (2. 10) reduces to

$$\mathcal{G}(\Psi)=\Lambda_0+\Lambda_1\Pi(\Psi)+\Lambda_2\Pi^2(\Psi), \tag{2. 11}$$

where Λ_0, Λ_1, and Λ_2 are unknown constants. The auxiliary function $\Pi(\Psi)$ satisfies the first-order nonlinear ordinary differential equation

$$\Pi'(\Psi) = \ln(\nu)\left(d_1 + d_2\Pi(\Psi) + d_3\Pi^2(\Psi)\right), \tag{2. 12}$$

where $\nu \neq 0, 1$, while d_1, d_2, and d_3 are arbitrary parameters.

Step 4: Substituting Eqs. (2. 11) and (2. 12) into Eq. (2. 9), followed by collecting the coefficients of identical powers of $\Pi(\Psi)$, yields a system of nonlinear algebraic equations. Solving this system symbolically, for example by using Maple, determines the unknown constants and leads to the corresponding exact analytical solutions.

$$\begin{cases} \Pi^{0J}(\Psi) & : Bk^4\left(\Lambda_1 d_2 d_1 \ln(v)^2 + 2\,\Lambda_2 {d_1}^2 \ln(v)^2\right) + (-k\omega + P)\,\Lambda_0 + \\ & \quad \frac{1}{2}Ak^2{\Lambda_0}^2 = 0, \\ \Pi^{1J}(\Psi) & : Bk^4\left(\Lambda_1\left(2\,\ln(v)^2 d_3 d_1 + \ln(v)^2 {d_2}^2\right) + 6\,\Lambda_2 d_2 d_1 \ln(v)^2\right) \\ & \quad + (-k\omega + P)\,\Lambda_1 + Ak^2\Lambda_0\Lambda_1 = 0, \\ \Pi^{2J}(\Psi) & : Bk^4\left(3\,\Lambda_1 d_2 \ln(v)^2 d_3 + 4\,\Lambda_2\left(2\,\ln(v)^2 d_3 d_1 + \ln(v)^2 {d_2}^2\right)\right) + \\ & \quad (-k\omega + P)\,\Lambda_2 + \frac{1}{2}Ak^2\left(2\,\Lambda_0\Lambda_2 + {\Lambda_1}^2\right) = 0, \\ \Pi^{3J}(\Psi) & : Bk^4\left(2\,\Lambda_1 \ln(v)^2 {d_3}^2 + 10\,\Lambda_2 d_2 \ln(v)^2 d_3\right) + Ak^2\Lambda_1\Lambda_2 = 0, \\ \Pi^{4J}(\Psi) & : 6\,Bk^4\Lambda_2 \ln(v)^2 {d_3}^2 + \frac{1}{2}Ak^2{\Lambda_2}^2 = 0. \end{cases}$$

The unknown coefficients are obtained by symbolically solving the corresponding algebraic equations. All symbolic manipulations and computational simplifications are carried out using Maple 2025.2. The resulting parameter values are expressed as:
$\Lambda_0 = -\frac{2Bk^2\ln(v)^2\left(2\,d_1 d_3 + {d_2}^2\right)}{A}, \Lambda_1 = -\frac{12Bk^2\ln(v)^2 d_2 d_3}{A}, \Lambda_2 = -\frac{12Bk^2\ln(v)^2 {d_3}^2}{A}$.
By inserting these parameter values into Eq. (2. 11) and subsequently employing the traveling-wave transformation defined in Eq. (2. 8), the exact solutions corresponding to Eq. (2. 7) are obtained as follows:
Case 1: If $\Delta = d_2^2 - 4d_3d_1 < 0$ and $d_3 \neq 0$, then

$$\left\{\begin{aligned}
\mathcal{F}_1(x,y,z,s,t) &= \tfrac{Bk^2(\ln v)^2}{A}(3\Delta\tan^2_\nu(\tfrac{\sqrt{-\Delta}\Psi}{2} - 4d_1d_3 + d_2^2),\\
\mathcal{F}_2(x,y,z,s,t) &= \tfrac{Bk^2(\ln v)^2}{A}(3\Delta\cot^2_\nu(\tfrac{\sqrt{-\Delta}\Psi}{2}) - 4d_1d_3 + d_2^2),\\
\mathcal{F}_3(x,y,z,s,t) &= \tfrac{Bk^2(\ln v)^2\Delta}{A}(3rs\ \sec^2_\nu(\sqrt{-\Delta}\Psi)\\
&\quad +6\sqrt{rs}\ \tan_\nu(\sqrt{-\Delta}\Psi)\sec_\nu(\sqrt{-\Delta}\Psi)\\
&\quad +3\tan^2_\nu(\sqrt{-\Delta}\Psi)) + \tfrac{Bk^2(\ln v)^2}{A}(-4d_1d_3 + d_2^2),\\
\mathcal{F}_4(x,y,z,s,t) &= \tfrac{Bk^2(\ln v)^2\Delta}{A}(3rs\ \csc^2_\nu(\sqrt{-\Delta}\Psi)\\
&\quad +6\sqrt{rs}\ \cot_\nu(\sqrt{-\Delta}\Psi)\csc_\nu(\sqrt{-\Delta}\Psi)\\
&\quad +3\cot^2_\nu(\sqrt{-\Delta}\Psi)) + \tfrac{Bk^2(\ln v)^2}{A}(-4d_1d_3 + d_2^2),\\
\mathcal{F}_5(x,y,z,s,t) &= \tfrac{Bk^2(\ln v)^2\Delta}{4A}(3\tan^2_\nu(\tfrac{\sqrt{-\Delta}\Psi}{4})\\
&\quad -6\tan_\nu(\tfrac{\sqrt{-\Delta}\Psi}{4})\cot_\nu(\tfrac{\sqrt{-\Delta}\Psi}{4})\\
&\quad +3\cot^2_\nu(\tfrac{\sqrt{-\Delta}\Psi}{4})) + \tfrac{Bk^2(\ln v)^2}{4A}(-16d_1d_3 + 4d_2^2).
\end{aligned}\right. \tag{2. 13}$$

Case 2: If $\Delta = d_2^2 - 4d_3d_1 > 0$ and $d_3 \neq 0$, then

$$\left\{\begin{aligned}
\mathcal{F}_6(x,y,z,s,t) &= -\tfrac{Bk^2(\ln v)^2}{A}(3\Delta\tanh^2_\nu(\tfrac{\sqrt{\Delta}\Psi}{2}) + 4d_1d_3 - d_2^2),\\
\mathcal{F}_7(x,y,z,s,t) &= -\tfrac{Bk^2(\ln v)^2}{A}(3\Delta\coth^2_\nu(\tfrac{\sqrt{\Delta}\Psi}{2}) + 4d_1d_3 - d_2^2),\\
\mathcal{F}_8(x,y,z,s,t) &= -\tfrac{Bk^2(\ln v)^2\Delta}{A}(3rs\ \mathrm{sech}^2_\nu(\sqrt{\Delta}\Psi)\\
&\quad +6\sqrt{rs}\ \tanh_\nu(\sqrt{\Delta}\Psi)\,\mathrm{sech}_\nu(\sqrt{\Delta}\Psi)\\
&\quad +3\tanh^2_\nu(\sqrt{\Delta}\Psi)) - \tfrac{Bk^2(\ln v)^2}{A}(4d_1d_3 - d_2^2),\\
\mathcal{F}_9(x,y,z,s,t) &= -\tfrac{Bk^2(\ln v)^2\Delta}{A}(3rs\ \mathrm{csch}^2_\nu(\sqrt{\Delta}\Psi)\\
&\quad +6\sqrt{rs}\ \coth_\nu(\sqrt{\Delta}\Psi)\,\mathrm{csch}_\nu(\sqrt{\Delta}\Psi)\\
&\quad +3\coth^2_\nu(\sqrt{\Delta}\Psi)) - \tfrac{Bk^2(\ln v)^2}{A}(4d_1d_3 - d_2^2),\\
\mathcal{F}_{10}(x,y,z,s,t) &= -\tfrac{Bk^2(\ln v)^2\Delta}{4A}(3\tanh^2_\nu(\tfrac{\sqrt{\Delta}\Psi}{4})\\
&\quad +6\tanh_\nu(\tfrac{\sqrt{\Delta}\Psi}{4})\coth_\nu(\tfrac{\sqrt{\Delta}\Psi}{4})\\
&\quad +3\coth^2_\nu(\tfrac{\sqrt{\Delta}\Psi}{4})) - \tfrac{Bk^2(\ln v)^2}{4A}(16d_1d_3 - 4d_2^2).
\end{aligned}\right. \tag{2. 14}$$

Case 3: If $d_3d_1 > 0$ and $d_2 = 0$, then

$$\begin{cases} \mathcal{F}_{11}(x,y,z,s,t) &= -\frac{4Bk^2(\ln v)^2 d_1 d_3}{A}(3\tan_\nu^2(\sqrt{d_1d_3}\Psi)+1), \\ \mathcal{F}_{12}(x,y,z,s,t) &= -\frac{4Bk^2(\ln v)^2 d_1 d_3}{A}(3\cot_\nu^2(\sqrt{d_1d_3}\Psi)+1), \\ \mathcal{F}_{13}(x,y,z,s,t) &= -\frac{4Bk^2(\ln v)^2 d_1 d_3}{A}(3rs\ \sec_\nu^2(2\sqrt{d_1d_3}\Psi) \\ & \quad +6\sqrt{rs}\ \sec_\nu(2\sqrt{d_1d_3}\Psi)\tan_\nu(2\sqrt{d_1d_3}\Psi) \\ & \quad +3\tan_\nu^2(2\sqrt{d_1d_3}\Psi)+1), \\ \mathcal{F}_{14}(x,y,z,s,t) &= -\frac{4Bk^2(\ln v)^2 d_1 d_3}{A}(3rs\ \csc_\nu^2(2\sqrt{d_1d_3}\Psi) \\ & \quad -6\sqrt{rs}\ \csc_\nu(2\sqrt{d_1d_3}\Psi)\cot_\nu(2\sqrt{d_1d_3}\Psi) \\ & \quad +3\cot_\nu^2(2\sqrt{d_1d_3}\Psi)+1), \\ \mathcal{F}_{15}(x,y,z,s,t) &= -\frac{Bk^2(\ln v)^2 d_1 d_3}{A}(3\tan_\nu^2(\frac{\sqrt{d_1d_3}\Psi}{2}) \\ & \quad -6\tan_\nu(\frac{\sqrt{d_1d_3}\Psi}{2})\cot_\nu(\frac{\sqrt{d_1d_3}\Psi}{2}) \\ & \quad +3\cot_\nu^2(\frac{\sqrt{d_1d_3}\Psi}{2})+4). \end{cases} \tag{2. 15}$$

Case 4: If $d_3d_1 < 0$ and $d_2 = 0$, then

$$\begin{cases} \mathcal{F}_{16}(x,y,z,s,t) &= \frac{4Bk^2\ \ln(v)^2 d_1 d_3 (3\ \tanh_\nu\left(\sqrt{-d_1d_3}(\Psi)\right)^2-1)}{A}, \\ \mathcal{F}_{17}(x,y,z,s,t) &= \frac{4Bk^2\ \ln(v)^2 d_1 d_3 (3\ \coth_\nu\left(\sqrt{-d_1d_3}(\Psi)\right)^2-1)}{A}, \\ [3pt]\mathcal{F}_{18}(x,y,z,s,t) &= \frac{4Bk^2\ \ln^2(v) d_1 d_3}{A}(3rs\ \text{sech}_\nu^2(2\sqrt{-d_1d_3}\ \Psi)+ \\ & \quad 6\sqrt{rs}\ \text{sech}_\nu(2\sqrt{-d_1d_3}\ \Psi)\tanh_\nu(2\sqrt{-d_1d_3}\ \Psi) \\ & \quad +3\tanh_\nu^2(2\sqrt{-d_1d_3}\ \Psi)-1), \\ \mathcal{F}_{19}(x,y,z,s,t) &= \frac{4Bk^2\ \ln^2(v) d_1 d_3}{A}(3rs\ \text{csch}_\nu^2(2\sqrt{-d_1d_3}\ \Psi)+ \\ & \quad 6\sqrt{rs}\ \text{csch}_\nu(2\sqrt{-d_1d_3}\ \Psi)\coth_\nu(2\sqrt{-d_1d_3}\ \Psi)+ \\ & \quad 3\coth_\nu^2(2\sqrt{-d_1d_3}\ \Psi)-1), \\ \mathcal{F}_{20}(x,y,z,s,t) &= -\frac{Bk^2\ \ln^2(v) d_1 d_3}{A}(3\tanh_\nu^2(\frac{\sqrt{-d_1d_3}\ \Psi}{2})+ \\ & \quad 6\tanh_\nu(\frac{\sqrt{-d_1d_3}\ \Psi}{2})\coth_\nu(\frac{\sqrt{-d_1d_3}\ \Psi}{2}) \\ & \quad +3\coth_\nu^2(\frac{\sqrt{-d_1d_3}\ \Psi}{2})-4). \end{cases} \tag{2. 16}$$

Case 5: If $d_2 = 0$ and $d_3 = d_1$, then

$$\begin{cases} \mathcal{F}_{21}(x,y,z,s,t) & = -\frac{4Bk^2(\ln(v))^2 {d_1}^2\left(3\left(\tan_\nu(d_1(\Psi))\right)^2+1\right)}{A}, \\ \mathcal{F}_{22}(x,y,z,s,t) & = -\frac{4Bk^2(\ln(v))^2 {d_1}^2\left(3\left(\cot_\nu(d_1(\Psi))\right)^2+1\right)}{A}, \\ \mathcal{F}_{23}(x,y,z,s,t) = & -\frac{4Bk^2(\ln v)^2 d_1^2}{A}(3rs\ \sec^2_\nu(2d_1(\Psi))+ \\ & 6\sqrt{rs}\ \tan_\nu(2d_1(\Psi))\sec_\nu(2d_1(\Psi))+3\tan^2_\nu(2d_1(\Psi))+1), \\ \mathcal{F}_{24}(x,y,z,s,t) = & -\frac{4Bk^2(\ln v)^2 d_1^2}{A}(3rs\ \csc^2_\nu(2d_1(\Psi))- \\ & 6\sqrt{rs}\ \cot_\nu(2d_1(\Psi))\csc_\nu(2d_1(\Psi))+3\cot^2_\nu(2d_1(\Psi))+1), \\ \mathcal{F}_{25}(x,y,z,s,t) & = -\frac{12\left(\frac{1}{2}tan_\nu\left(\frac{1}{2}\,d_1(\Psi)\right)-\frac{1}{2}\ \cot_\nu\left(\frac{1}{2}\,d_1(\Psi)\right)\right)^2 Bk^2(\ln(v))^2{d_1}^2}{A}- \\ & \frac{4Bk^2(\ln(v))^2{d_1}^2}{A}. \end{cases} \tag{2. 17}$$

Case 6: If $d_2 = 0$ and $d_3 = -d_1$, then

$$\begin{cases} \mathcal{F}_{26}(x,y,z,s,t) & = -\frac{4Bk^2(\ln v)^2 d_1^2}{A}(3\tanh^2_\nu(d_1\Psi)-1), \\ \mathcal{F}_{27}(x,y,z,s,t) & = -\frac{4Bk^2(\ln v)^2 d_1^2}{A}(3\coth^2_\nu(d_1\Psi)-1), \\ \mathcal{F}_{28}(x,y,z,s,t) & = -\frac{4Bk^2(\ln v)^2 d_1^2}{A}(3rs\ \mathrm{sech}^2_\nu(2d_1\Psi) \\ & -6\sqrt{rs}\ \tanh_\nu(2d_1\Psi)\,\mathrm{sech}_\nu(2d_1\Psi) \\ & +3\tanh^2_\nu(2d_1\Psi)-1), \\ \mathcal{F}_{29}(x,y,z,s,t) & = -\frac{4Bk^2(\ln v)^2 d_1^2}{A}(3rs\ \mathrm{csch}^2_\nu(2d_1\Psi) \\ & -6\sqrt{rs}\ \coth_\nu(2d_1\Psi)\,\mathrm{csch}_\nu(2d_1\Psi) \\ & +3\coth^2_\nu(2d_1\Psi)-1), \\ \mathcal{F}_{30}(x,y,z,s,t) & = -\frac{12Bk^2(\ln v)^2 d_1^2}{A}(-\frac{1}{2}\tanh_\nu\left(\frac{d_1\Psi}{2}\right)-\frac{1}{2}\coth_\nu\left(\frac{d_1\Psi}{2}\right))^2 \\ & +\frac{4Bk^2(\ln v)^2 d_1^2}{A}. \end{cases} \tag{2. 18}$$

Case 7: If $d_2^2 = 4d_3d_1$, then

$$\begin{cases} \mathcal{F}_{31}(x,y,z,s,t) & = -\frac{3Bk^2}{Ad_1^2\Psi^2}(4(\ln v)^2\Psi^2 d_1^3 d_3 \\ & -4d_1\left(2\sqrt{d_1d_3}\Psi\ln(v)+2\right)\sqrt{d_1d_3}\ln(v)\Psi \\ & +d_1\left(2\sqrt{d_1d_3}\Psi\ln(v)+2\right)^2). \end{cases} \tag{2. 19}$$

Case 8: If $d_2 = \lambda,\ d_1 = p\lambda\ (p \neq 0)$ and $d_3 = 0$, then

$$\mathcal{F}_{32}(x,y,z,s,t) = -\frac{2Bk^2\left(\ln(v)\right)^2\lambda^2}{A}. \tag{2. 20}$$

Case 9: If $d_2 = d_3 = 0$, then

$$\mathcal{F}_{33}(x, y, z, s, t) = 0. \tag{2. 21}$$

Case 10: If $d_2 = d_1 = 0$, then

$$\mathcal{F}_{34}(x, y, z, s, t) = -\frac{12Bk^2}{A\Psi^2}. \tag{2. 22}$$

Case 11: If $d_1 = 0$ and $d_2 \neq 0$, then

$$\begin{cases} \mathcal{F}_{35}(x, y, z, s, t) & = -\frac{12Bk^2(\ln v)^2 r^2 d_2^2}{A(\cosh_\nu(d_2\Psi)-\sinh_\nu(d_2\Psi)+r)^2} \\ & \quad +\frac{12Bk^2(\ln v)^2 d_2^2 r}{A(\cosh_\nu(d_2\Psi)-\sinh_\nu(d_2\Psi)+r)} - \frac{2Bk^2(\ln v)^2 d_2^2}{A}, \\ \mathcal{F}_{36}(x, y, z, s, t) & = -\frac{2Bk^2(\ln v)^2 d_2^2}{A(\sinh_\nu(d_2\Psi)+\cosh_\nu(d_2\Psi)+s)^2}(\sinh_\nu^2(d_2\Psi) \\ & \quad +2\sinh_\nu(d_2\Psi)\cosh_\nu(d_2\Psi) - 4s\sinh_\nu(d_2\Psi) \\ & \quad +\cosh_\nu^2(d_2\Psi) - 4s\cosh_\nu(d_2\Psi) + s^2). \end{cases} \tag{2. 23}$$

Case 12: If $d_2 = \lambda,\ d_3 = p\lambda$ and $d_1 = 0$, then

$$\begin{cases} \mathcal{F}_{37}(x, y, z, s, t) & = -\frac{12Bk^2(\ln(v))^2\lambda p^2\ rv^{2\,\lambda\Psi}}{A(s-\ prv^{\lambda\Psi})^2} - \frac{12Bk^2(\ln(v))^2\lambda\,\lambda p\ \ rv^{\lambda\Psi}}{A(s-\ prv^{\lambda\Psi})} - \\ & \frac{2Bk^2(\ln(v))^2\lambda^2}{A}. \end{cases} \tag{2. 24}$$

3. Graphical Representations of Soliton Wave Solutions.

This section presents the graphical visualization of the exact solutions obtained for Eq. (2. 7) using MATLAB (2018). The derived analytical solutions are represented through trigonometric, hyperbolic, and Jacobi elliptic functions, allowing a comprehensive examination of their propagation characteristics. Based on their distinct wave profiles, the solutions are classified into four categories: solitary waves, bright solitons, dark solitons, and periodic wave structures. Among these solution classes, the Jacobi elliptic solutions have some special interest due to the availability of exact analytical expressions, which are extensively used in nonlinear mathematical physics problems. Moreover, the bright soliton solutions portray highly concentrated, non-dispersive, shape-preserving wave packets that sustain amplitude and form as they pass through the nonlinear medium. Those are particularly suitable in high power and highly energetic events, including strong pulses in optical or physical settings. The bright solitons are stable, and they provide useful results in nonlinear optics and plasma media where the transmission of high pulses is an essential aspect. Unlike bright solitons, the dark solitons reflect an amplitude or intensity depression that appears at isolated spots in a continuous wave background. The solutions are usually confined to a low-intensity level regime, and they help study nonlinear wave propagation when events carry a small amount of energy. This has been applied in optical waves in a plasma and in some low-energy regimes. Bright and dark solitons help understanding of the structure of equation of states, the Eq. (2. 7) that it is often assumed a part of. We found a regular oscillatory solution of the type of a constant train of small oscillations. On the other hand, the presence of the so-called singular solutions means we have a kind of critical condition for some variable for which the mathematical expression explodes. Although in reality these phenomena cannot happen, sometimes it can be of interest for the limitations of our numerical algorithms and the use of analytical and numeric modeling of nonlinear wave propagation problems. The corresponding wave structures are summarized in Table (1).

TABLE 1. Graphical representation of soliton solutions with corresponding parameters and wave behaviors.

Fig.	Solution	Equation Ref.	Parameters	Wave Behavior
2	$\mathcal{F}_1(x,y,z,s,t)$	Eq. (2. 13)	$d_1 = 1$, $d_2 = 3$, $d_3 = 3$, $v = 3$, $\Delta = d_2^2 - 4d_1d_3$, $m = 1$, $k = 1$, $\omega = 1$, $y = 0$, $s = 0$, $n = 1$, $s_1 = 1$, $r = 1$, $A = 2$, $B = 3$, $z = 0$	Periodic wave
3	$\mathcal{F}_3(x,y,z,s,t)$	Eq. (2. 13)	$d_1 = 1$, $d_2 = 3$, $d_3 = 3$, $v = 3$, $\Delta = d_2^2 - 4d_1d_3$, $m = 1$, $k = 1$, $\omega = 1$, $y = 0$, $s = 0$, $n = 1$, $s_1 = 1$, $r = 1$, $A = 2$, $B = 3$, $z = 0$	Multiple singular wave solution
4	$\mathcal{F}_6(x,y,z,s,t)$	Eq. (2. 14)	$d_1 = 1$, $d_2 = 3$, $d_3 = 1$, $v = 3$, $\Delta = d_2^2 - 4d_1d_3$, $m = 1$, $k = 1$, $\omega = 1$, $y = 0$, $s = 0$, $n = 1$, $s_1 = 1$, $r = 1$, $A = 2$, $B = 3$, $z = 0$	Bright wave solution
5	$\mathcal{F}_7(x,y,z,s,t)$	Eq. (2. 14)	$d_1 = 1$, $d_2 = 3$, $d_3 = 3$, $v = 3$, $\Delta = d_2^2 - 4d_1d_3$, $m = 1$, $k = 1$, $\omega = 1$, $y = 0$, $s = 0$, $n = 1$, $s_1 = 1$, $r = 1$, $A = 2$, $B = 3$, $z = 0$	Dark wave solution
6	$\mathcal{F}_{26}(x,y,z,s,t)$	Eq. (2. 18)	$d_1 = 2$, $d_2 = 0$, $d_3 = -2$, $v = 3$, $\Delta = d_2^2 - 4d_1d_3$, $m = 1$, $k = 1$, $\omega = 1$, $y = 0$, $s = 0$, $n = 1$, $s_1 = 1$, $r = 1$, $A = 2$, $B = 3$, $z = 0$	Kink wave solution

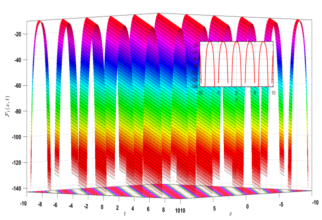

(a) 3D Graph

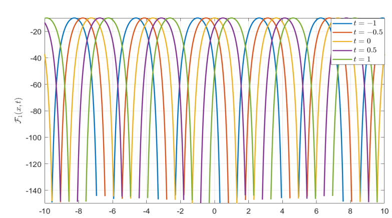

(b) 2D Graph

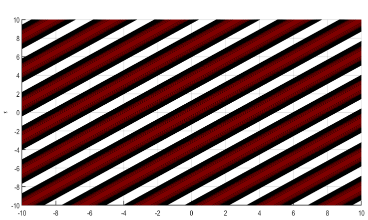

(c) Contour Graph

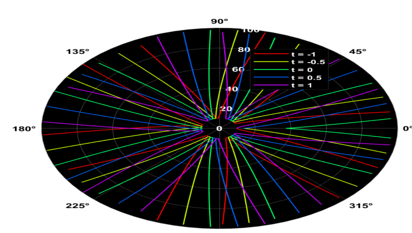

(d) Polar Graph

FIGURE 2. Periodic wave behavior of $\mathcal{F}_1(x,t)$ for an appropriate choice of the model parameters.

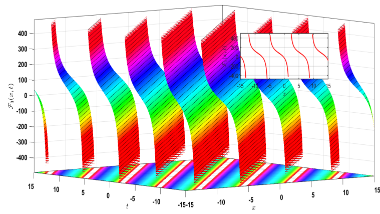

(a) 3D Graph

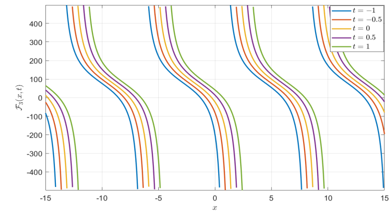

(b) 2D Graph

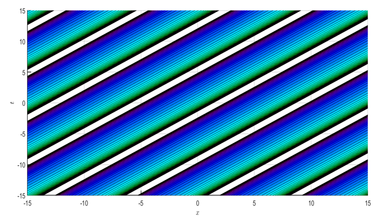

(c) Contour Graph

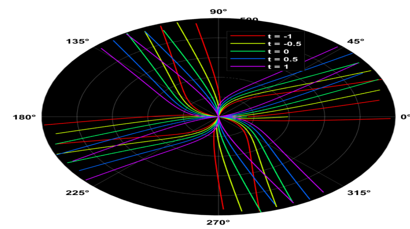

(d) Polar Graph

FIGURE 3. Multiple singular wave behavior of $\mathcal{F}_3(x,t)$ for an appropriate choice of the model parameters.

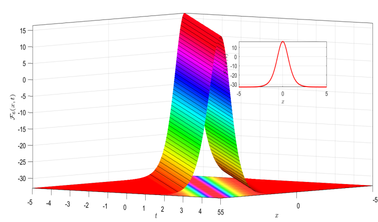

(a) 3D Graph

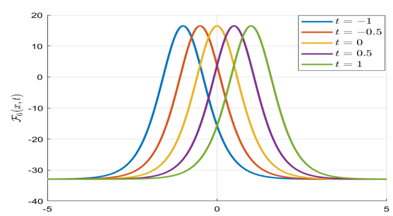

(b) 2D Graph

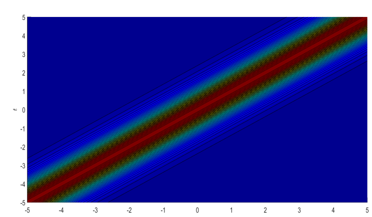

(c) Contour Graph

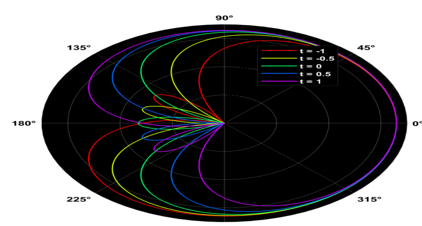

(d) Polar Graph

FIGURE 4. Shows bright wave behavior for $\mathcal{F}_6(x,t)$ with the help of suitable the parameters.

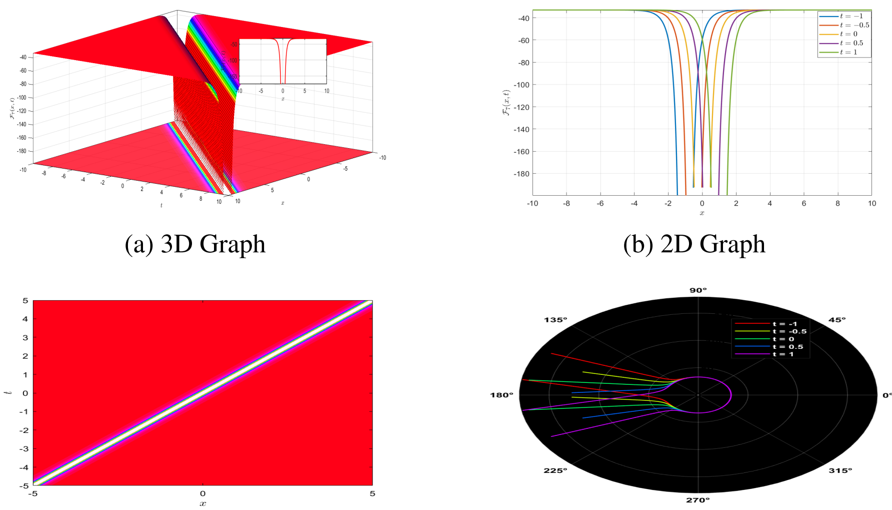

(a) 3D Graph (b) 2D Graph

(c) Contour Graph (d) Polar Graph

FIGURE 5. Shows dark wave behavior for $\mathcal{F}_7(x,t)$ With the suitable parameters.

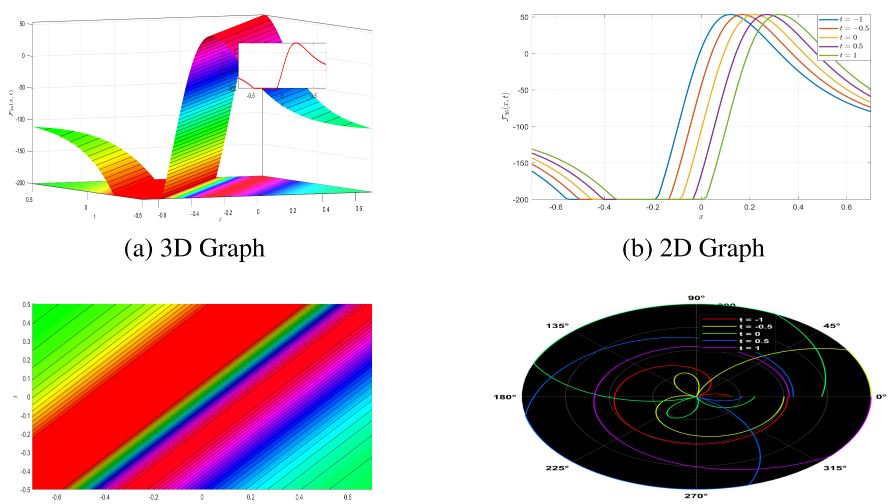

(a) 3D Graph (b) 2D Graph

(c) Contour Graph (d) Polar Graph

FIGURE 6. Shows kink wave behavior for $\mathcal{F}_{26}(x,t)$ with the suitable parameters.

4. DYNAMICAL ANALYSIS

Dynamical analysis is a powerful method used to study the behavior of the system at issue over time. By using various techniques such as the phase portraits, the bifurcation diagrams and the LEs to discover the fixed point (which are called equilibria), evaluate the stability of the latter as well as identify complex dynamical behavior like oscillations, periodicity or chaos. The analysis of dynamics is thus particularly interesting for nonlinear systems where the slightest variation in ICs or parameter leads to very different dynamics.

4.1. **Phase Portrait Analysis of the Model.** The study of the time development of dynamical systems with the help of phase portrait offers a powerful methodological approach to this problem, consisting of graphical representations. According to this method, the system trajectories are plotted in phase space, with each of the axes being a fundamental state variable of the system used as the axis of the phase space diagrams [29]. This kind of representation allows one to discover a clear representation of important dynamical properties, such as equilibrium states, stability properties, periodic orbits, and chaotic dynamics. The key benefit of phase portraits is that despite the problems associated with finding accurate analytical solutions, they can provide qualitative information about the dynamics of a system. Due to this ability, the phase portrait analysis has become a vital instrument in most fields of science, such as physics, engineering, and biology. To formulate the associated dynamical system, a Galilean transformation is employed. By introducing the variables $\mathcal{G}' = \mathcal{H}$ and $\mathcal{G}'' = \mathcal{H}'$, the governing equation can be rewritten in the following dynamical system form:

$$\begin{cases} \frac{d\mathcal{G}}{d\Psi} = \mathcal{H}, \\ \frac{d\mathcal{H}}{d\Psi} = \gamma_0\mathcal{G} - \gamma_1\mathcal{G}^2. \end{cases} \tag{4. 25}$$

where $\gamma_0 = \dfrac{\omega k - P}{Bk^4}$ and $\gamma_1 = \dfrac{A}{2Bk^2}$. The Jacobian matrix corresponding to system (4. 25) is given by

$$det(\mathcal{J}(\mathcal{G}, \mathcal{H})) = \begin{vmatrix} 0 & 1 \\ \gamma_0 - 2\gamma_1\mathcal{G} & 0 \end{vmatrix} = 2\gamma_1\mathcal{G} - \gamma_0. \tag{4. 26}$$

Equilibrium points occur where $\mathcal{G}' = 0$ and $\mathcal{H}' = 0$. So, we have

$$\gamma_0\mathcal{G} - \gamma_1\mathcal{G}^2 = 0, \quad and \quad \mathcal{H} = 0.$$

By utilizing qualitative analysis, two equilibrium points for the preceding system of DEs are determined in the following form: $\mathcal{N}_1 = (0,\ 0), \mathcal{N}_2 = (\frac{\gamma_0}{\gamma_1},\ 0)$.
The stability and type of the equilibrium points are determined by the sign of the Jacobian determinant, as summarized in Table (2).

TABLE 2. Classification of equilibrium points based on the determinant of the Jacobian matrix

Equilibrium Type	Cuspid	Saddle	Center
$\lvert\mathcal{J}(\mathcal{G}, \mathcal{H})\rvert$	0	Negative	Positive

By assigning different values to the parameters that are involved, a variety of qualitative behaviors observed in the system. These results are summarized in Table (3).

TABLE 3. Equilibrium points and their nature under various parameter conditions

Case	Conditions	Equilibrium Points	Parameters (ω, B, k, A, P)	Nature of Equilibrium Points	Figure
1	$\gamma_0 > 0,\ \gamma_1 > 0$	$\mathcal{N}_1 = (0,0)$, $\mathcal{N}_2 = (2,0)$	$(9,1,1,8,1)$	$\mathcal{N}_1$: Saddle; $\mathcal{N}_2$: Center	Fig. 7(a)
2	$\gamma_0 < 0,\ \gamma_1 < 0$	$\mathcal{N}_1 = (0,0)$, $\mathcal{N}_2 = (2,0)$	$(1,1,1,-8,9)$	$\mathcal{N}_1$: Center; $\mathcal{N}_2$: Saddle	Fig. 7(b)
3	$\gamma_0 > 0,\ \gamma_1 < 0$	$\mathcal{N}_1 = (0,0)$, $\mathcal{N}_2 = (-2,0)$	$(-1,1,1,-8,-9)$	$\mathcal{N}_1$: Saddle; $\mathcal{N}_2$: Center	Fig. 7(c)
4	$\gamma_0 < 0,\ \gamma_1 > 0$	$\mathcal{N}_1 = (0,0)$, $\mathcal{N}_2 = (-1,0)$	$(1,1,1,8,5)$	$\mathcal{N}_1$: Center; $\mathcal{N}_2$: Saddle	Fig. 7(d)

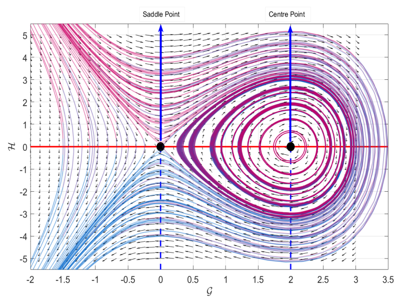

(a)Trajectory plot for $\gamma_0 > 0$ and $\gamma_1 > 0$.

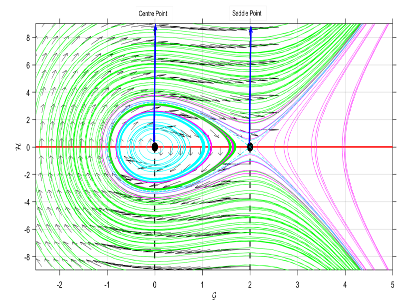

(b)Trajectory plot for $\gamma_0 > 0$ and $\gamma_1 < 0$.

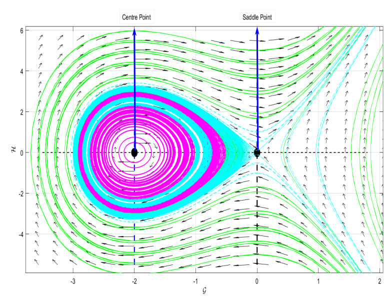

(c)Trajectory plot for $\gamma_0 < 0$ and $\gamma_1 > 0$.

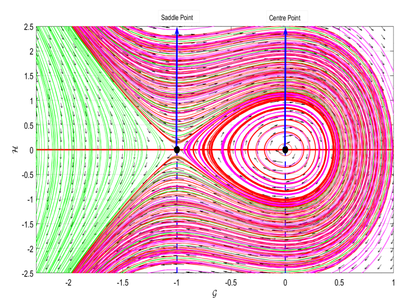

(d)Trajectory plot for $\gamma_0 < 0$ and $\gamma_1 < 0$.

FIGURE 7. Graphical representation of system's trajectories of system (4. 25)

4.2. Analysis of Phase Portraits Trajectories.

Behavior of Phase Plot for $\gamma_0 > 0$ and $\gamma_1 > 0$. In Fig. 7(a), the phase portrait shows a center point on the right, around which trajectories form concentric closed orbits. This indicates that the motion stays within stable periodic oscillations. A saddle point is on the left, and it makes separatrix curves that split the phase plane into several dynamic areas. Trajectories that start near the center stay in stable loops, whereas those that start near the saddle are pushed out in unstable directions.

Behavior of Phase Plot for $\gamma_0 > 0$ and $\gamma_1 < 0$. Fig. 7(b) shows that the center point is located at the left hand side of the phase plane, and there are closed orbits around the center point such that, a stable oscillatory region is created. A saddle point is used to regulate the unstable dynamics on the right. Separatrixes are used to differentiate restricted trajectories and the divergent ones. The alteration of the sign of the $\gamma_0 > 0$ alters the arrangement that was used in the previous example and is a kind of inverting the structure.

Behavior of Phase Plot for $\gamma_0 < 0$ and $\gamma_1 > 0$. Fig. 7(c) shows that the center point is located on the left side of the phase plane and closed circles are drawn around the center to give a steady oscillatory region. On the right, there is a saddle point that controls the unstable dynamics and separatrixes that differentiate between the bounded and the divergent trajectories. The fact that the sign of the value of $\gamma_0 > 0$ is reversed in the second time transforms the pattern to the initial drawing, which is to invert the structure.

Behavior of Phase Plot for $\gamma_0 < 0$ and $\gamma_1 < 0$. Fig. 7(d) indicates that the center point is at the right side and is enclosed by close trajectories that are nested indicating that the oscillations are stable and periodic. To the left, a saddle point is formed which forms unstable separatrix curves, expelling the trajectories. The case is identical to the trend observed in Fig. 7(c) though with the positions of the equilibrium points being swapped since the two parameters are negative.

4.3. **Chaotic Phenomena.** Chaos refers to the emergence of highly complex and seemingly irregular behavior in deterministic dynamical systems, primarily due to their strong sensitivity to initial conditions. Although such systems are governed by well-defined mathematical laws, their long-term evolution may appear random and unpredictable. One of the most famous examples of this phenomenon is the butterfly effect in which even a slight change in the starting point can cause very different results to appear in the end result. The nature of chaotic systems is so that they are non-periodic, they do not repeat themselves as time goes on. However their movement is confined and has a structured nature and in many cases it tends to take some complex geometry shapes referred to as strange attractors in phase space. There are chaotic systems that can be seen in a variety of natural and applied systems such as atmospherics, population models, and fluid flows. In this section, we analyze the periodic, quasi-periodic, and chaotic responses exhibited by the proposed model. To examine the influence of periodic excitation on the system dynamics, a harmonic forcing term, $\kappa_0 \cos(\omega\Psi)$, is introduced into system (4. 25). In this expression, κ_0 specifies the forcing amplitude, whereas ω corresponds to the excitation frequency. Consequently, system (4. 25) is reformulated as

$$\begin{cases} \frac{d\mathcal{G}}{d\Psi} = \mathcal{H}, \\ \frac{d\mathcal{H}}{d\Psi} = \gamma_0\mathcal{G} - \gamma_1\mathcal{G}^2 + \kappa_0\cos(\mathcal{M}), \\ \frac{d\mathcal{M}}{d\Psi} = \omega. \end{cases} \tag{4. 27}$$

Where $\mathcal{M} = \omega\Psi$. We examine periodic, quasi-periodic, and chaotic behaviors to find out how system (4. 27) behaves over time, with the help of time evolution graphs, 2D phase plots, and 3D phase portraits. We change the values of the parameters external force amplitude (κ_0) and external frequency (ω) while leaving the other parameters at $\gamma_0 = -2$ and

$\gamma_1 = 0.5$ as given in Table (4).

TABLE 4. System behavior for varying fxternal force amplitude κ_0 and frequency ω.

Case	κ_0	ω	**Behavior**	**Description**
1	0.005	0.2	Periodic	Regular and repetitive motion due to low external force and frequency; motion is stable. (Fig. 8)
2	0.3	0.8	Quasi-periodic	Motion begins to deviate from exact repetition but remains smooth and bounded; early signs of complexity. (Fig. 9)
3	0.8	π	Quasi-periodic	Increased amplitude and frequency cause more complex paths that remain non-chaotic but non-repeating. (Fig. 10)
4	1.8	2π	Chaotic	Strong nonlinear response leads to irregular, sensitive, and unpredictable motion. Paths exhibit randomness. (Fig. 11)

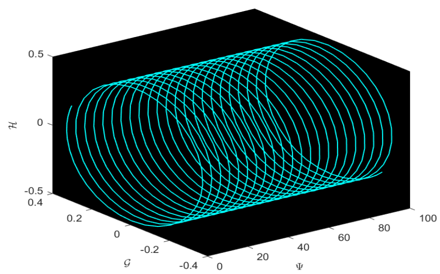

(a)3D Plot.

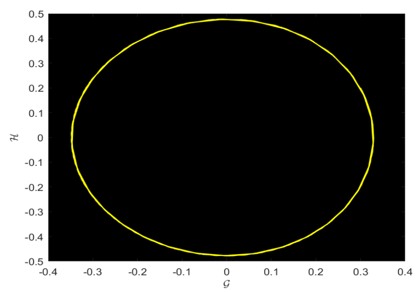

(b) 2D Plot.

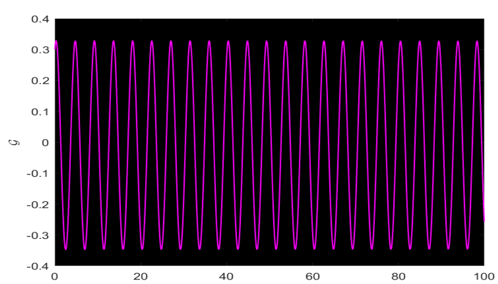

(c)Time series Plot

FIGURE 8. Three and three-dimensional graphs of system (4. 27) corresponding to $\kappa_0 = 0.005$ and $\omega = 0.2$, demonstrating the stable periodic motion under the influence of parameter variation.

Analysis of Periodic Behavior in Fig. (8). The Fig. (8) demonstrates a periodic wave influenced by the parameters $\gamma_0 = -2$, $\gamma_1 = 0.5$, $\kappa_0 = 0.005$ and $\omega = 0.2$. The magenta curve depicts the time series at a given spatial position and this depicts periodic oscillations which are characteristic of time periodicity. Spatial cross-section is given by the yellow curve and shows the repetitive structure of the wave whereas the surface given by the cyan color shows the complete spatiotemporal dynamics of the wave that are in stable form of a soliton. Such a behavior is a real-life example of such phenomena as the waves of water in a canal, the period variation of voltages across nonlinear LC circuits, or stable light pulses in a fiber, where the amplitude and periodicity are maintained with time and space.

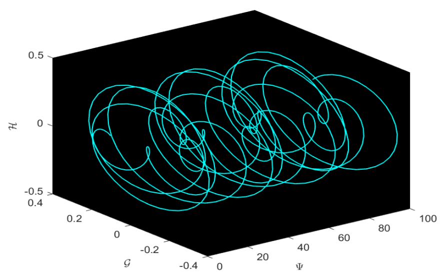

(a)3D Plot.

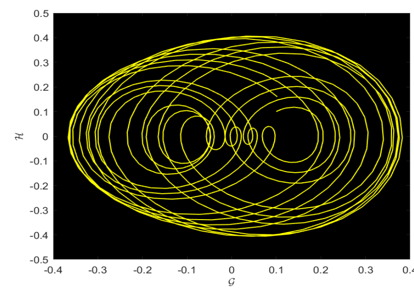

(b) 2D Plot.

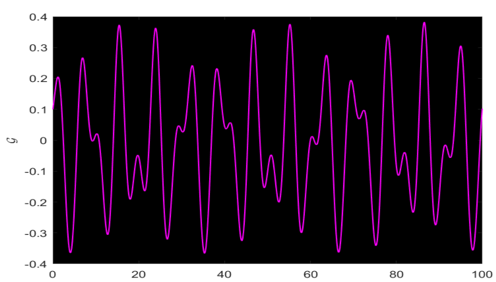

(c)Time series Plot

FIGURE 9. Three and two-dimensional portraits of system (4. 27) for $\kappa_0 = 0.3$ and $\omega = 0.8$, confirming the presence of quasi-periodic behavior through bounded, non-repeating trajectories in phase space.

Analysis of Quasi-Periodic Behavior in Fig. (9). The Fig. (9) illustrates a quasi-periodic wave structure arising from the parameters $\gamma_0 = -2$, $\gamma_1 = 0.5$, $\kappa_0 = 0.3$, and $\omega = 0.8$. The magenta curve shows time series at a given spatial point with disorganized oscillations with different peaks which is typical of a quasi-periodicity. The yellow curve is a spatial profile of a 2D profile at one instant in time, and shows minor distortions of perfect periodicity because of a number of interacting frequencies. The 3D spatiotemporal evolution is fully manifested in the cyan surface, where it is observed that the patterns of ridges have different amplitude and spacing. This behavior is typical of nonlinear systems that are driven at a number of different frequencies and is seen in real-life processes such as interacting ocean waves, nonlinear optical pulses, electrical circuits with many oscillators and quasi-periodic planetary motions.

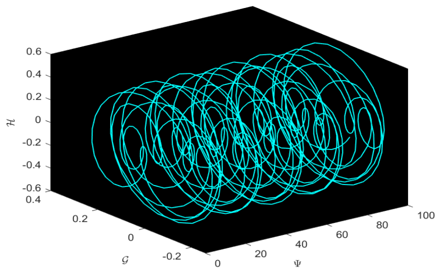

(a)3D Plot.

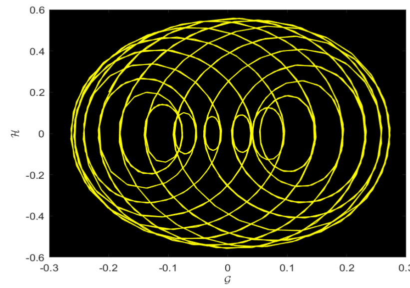

(b) 2D Plot.

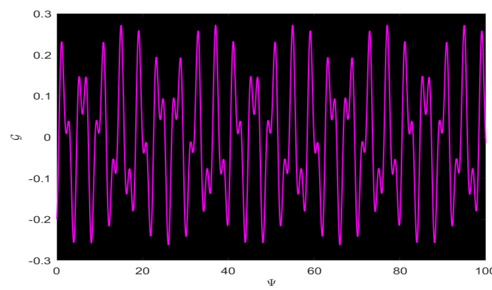

(c)Time series Plot

FIGURE 10. Three and two dimensional graphs of system (4. 27) for $\kappa_0 = 0.8$ and $\omega = \pi$, illustrating quasi-periodic dynamical behavior.

Analysis of Transition from Qausi periodic to Chaotic Behavior in Fig. (10). For the parameters $\kappa_0 = 0.8$ and $\omega = \pi$ with γ_0, γ_1 as in the graphs above, the system shows a clear cut-off transition to chaotic behavior. Under lower values, the system can also exhibit quasi-periodic oscillations, with uniform, regular phase space trajectories, however, at such high values, the dynamics become very sensitive to ICs. The orbits become irregular and non-recursive and fill the phase space in a complicated, non-periodic manner which are typical of chaos. The time series is presented in magenta curve, the 2D phase portrait in the yellow curve, and the surface in cyan color in the visual representation, respectively, and the irregular variations with time, the aperiodic trajectories on the plane, as well as the complex structure of the chaotic attractor, respectively. An example in real life can be provided by weather patterns: when weather is mild, climate would be regularly predicted and any slight variation in factors such as temperature or pressure can cause very unpredictable changes such as sudden storms or turbulence just like the system develops a quasi-periodic to chaotic behavior as the intensity and frequency of the weather increases.

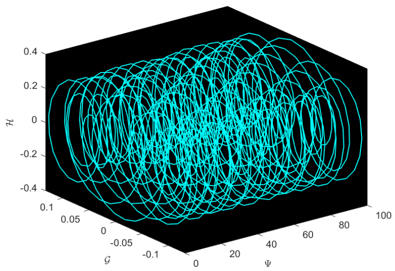

(a)3D Plot.

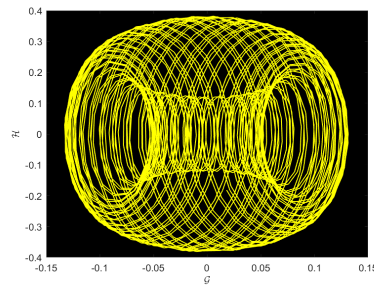

(b) 2D Plot.

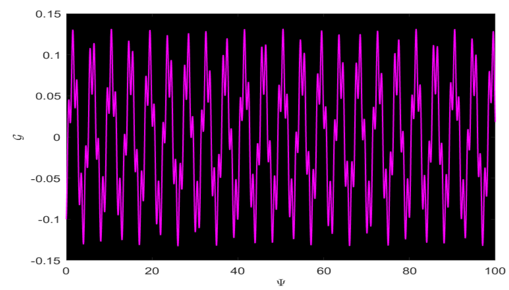

(c)Time series Plot

FIGURE 11. Three and two dimensional graphs of system (4. 27) for $\kappa_0 = 1.8$ and $\omega = 2\pi$, confirming the manifestation of chaotic dynamics through highly irregular, bounded trajectories in phase space.

Analysis of Chaotic Behavior in Fig. (11). The Fig. (11) shows that the system passes into a phase of entirely developed chaotic dynamics at the value of $\kappa_0 = 1.8$ and $\omega = 2\pi$, with γ_0 and γ_1 as shown in the above graphs. It is very irregular and aperiodic in nature and it is extremely sensitive to initial conditions such that the slightest deviations give vastly different trajectories. The time series in the visualizations is plotted in magenta, indicating the erratic time variations; the 2D phase plot in yellow, indicating the dense, tangled structure of the system, and the 3D trajectory in cyan, indicating the complex structure of the system, is plotted. This would be likened to turbulence of water in a river with a high flow whereby unpredictable swirling currents and eddies arise, as a result of the complex, intertwined structure in the phase space. These parameters propel the system much further than the quasi-periodic states and give rise to strong chaotic behavior which is both aesthetically compelling and dynamically abundant.

4.4. **Lyapunov Exponent.** Lyapunov exponents (LEs) provide a fundamental quantitative measure for characterizing the long-term behavior of nonlinear dynamical systems. They describe the mean exponential rates at which initially neighboring trajectories either separate or approach one another in phase space, thereby revealing the system's sensitivity to ICs. Unlike the local eigenvalues of the Jacobian matrix, which characterize the behavior only in the vicinity of equilibrium points, LEs capture the global dynamical evolution of trajectories. Consequently, they serve as an effective indicator for distinguishing periodic, quasi-periodic, and chaotic motions [24]. In this work, the Lyapunov spectrum is evaluated numerically using the Wolf algorithm in conjunction with the Gram–Schmidt orthogonalization technique. During the numerical integration, perturbation vectors are periodically orthonormalized to ensure numerical stability and to obtain reliable estimates of the LEs over long simulation times. Therefore, the reported LEs are obtained exclusively from the long-time evolution of the dynamical system and are not derived from the eigenvalues of the Jacobian matrix. Fig. (12) illustrates the temporal evolution of the LEs for different ICs and parameter sets. For the parameter values $(\gamma_0, \gamma_1) = (-2, 0.5)$ with the IC $(0.5, -0.6, 0.5)$, the LEs exhibit transient oscillations before converging to their asymptotic values. To ensure the convergence and reliability of the computed exponents, the numerical integration was performed over the time interval $t \in [1, 80]$. The resulting Lyapunov spectrum is $(\lambda_1, \lambda_2, \lambda_3) = (0.015693,\ 0,\ -0.015693)$. The positive largest LE confirms the exponential divergence of nearby trajectories and demonstrates sensitive dependence on ICs, the zero exponent corresponds to the direction of the system flow, and the negative exponent indicates contraction along the remaining phase-space direction. These numerical results provide strong evidence for the existence of a bounded chaotic attractor and verify the chaotic behavior of the perturbed dynamical system.

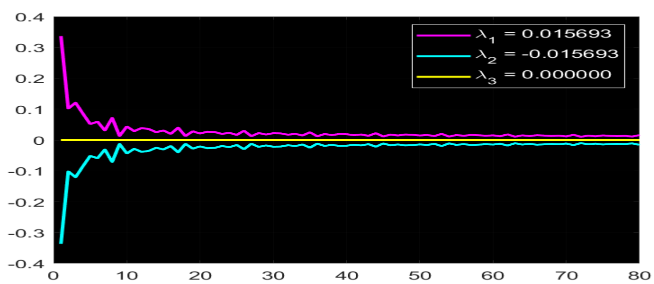

FIGURE 12. The Lyapunov spectrum $(\lambda_1, \lambda_2, \lambda_3) = (0.015693, -0.015693, 0)$ confirms chaotic dynamics, with one positive, one negative, and one zero exponent, indicating sensitive dependence on ICs.

4.5. **Poincaré Map.** A Poincaré map (PM) is a fundamental analytical tool in nonlinear dynamics that provides a reduced representation of the long-term behavior of a continuous dynamical system [31]. The construction is obtained by sampling a lower-dimensional surface, called the Poincaré section of the system's phase space, through successive encounters with a given system trajectory. By turning a continuous flow of a dynamical system in its phase space into a discrete series of points, the PM can capture main properties of high-dimensional dynamics while it helps reduce its complexity. Various types of dynamics can be directly analyzed due to their visual geometric location. In this view, periodic motion will yield one or a discrete, finite number of points, while quasi-periodic dynamics correspond to closed curves, and chaotic motion generates a complex spread of scattered points that exhibit a fractal nature. Since PM allows researchers to understand the system dynamics in terms of its stability, bifurcations, and the genesis of chaos, it has grown into a major tool for exploring nonlinear systems.

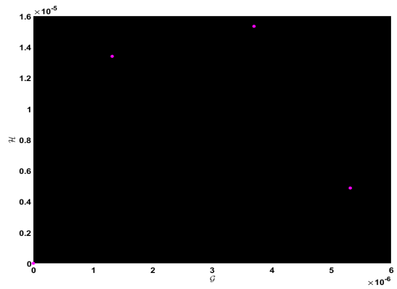

(a) Periodic behavior for $\kappa_0 = .0001$,and $\omega = .1$

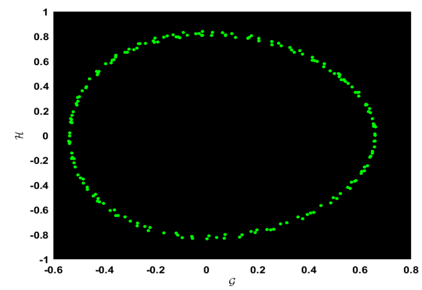

(b) Quasi-Periodic $\kappa_0 = 0.1$, and $\omega = 0.5$

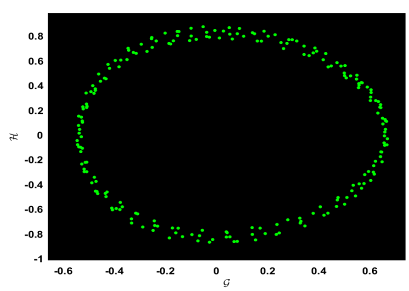

(c) Quasi-Periodic $\kappa_0 = 0.5$, and $\omega = \pi$

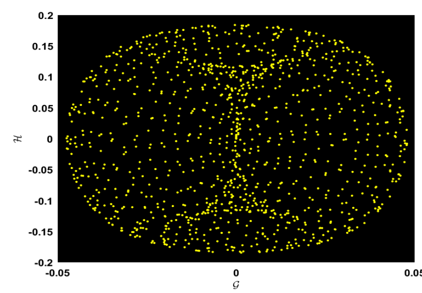

(d) Chaotic behavior $\kappa_0 = 2.5$, and $\omega = 2\pi$

FIGURE 13. Poincaré maps of system (4. 27) for fixed $\gamma_0 = -2$ and $\gamma_1 = 0.5$, revealing the transition from regular (periodic and quasi-periodic) to chaotic behavior induced by changes in the parameters κ_0 and ω.

4.6. **Multistability.** The purpose of this section is to investigate the arising of the multistable dynamics of system (4. 27), shown in Fig. (14). It is found that system displays the relatively high potentiality of multistability, it can support multiple kinds of states, periodic, quasi-periodic and chaotic, coexist under certain perturbations as a function of the selected ICs and parameter value. In Fig. 14(a), the system displays periodic dynamics for three different initial states: $(0.3, -0.2)$ in magenta, $(0.2, -0.2)$ in yellow, and $(0.3, -0.1)$ in green, with parameters $\gamma_0 = -2$, $\gamma_1 = 0.5$, $\kappa_0 = 0.005$, and $\omega = 0.2$. Fig. 14(b) shows quasi-periodic behavior under initial conditions $(0.3, -0.2)$, $(0.2, -0.2)$, and $(0.3, -0.1)$, with $\gamma_0 = -2$, $\gamma_1 = 0.5$, $\kappa_0 = 0.3$, and $\omega = 0.8$. In Fig. 14(c), the system again exhibits quasi-periodic motion for the same ICs with $\gamma_0 = -2$, $\gamma_1 = 0.5$, $\kappa_0 = 1.5$, and $\omega = \pi$. Finally, Fig. 14(d) demonstrates chaotic dynamics under ICs $(0.3, -0.2)$, $(0.2, -0.2)$, and $(0.3, -0.1)$, with $\gamma_0 = -2$, $\gamma_1 = 0.5$, $\kappa_0 = 2.5$, and $\omega = 2\pi$. Overall, these results indicate that even small variations in parameters and initial states can significantly alter the system's evolution, confirming its multistable nature.

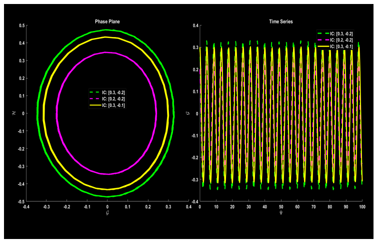

(a) Multistability Analysis

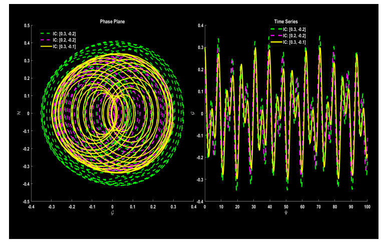

(b) Multistability Analysis

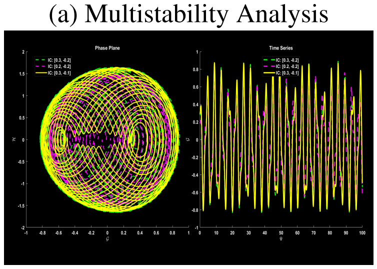

(c) Multistability Analysis

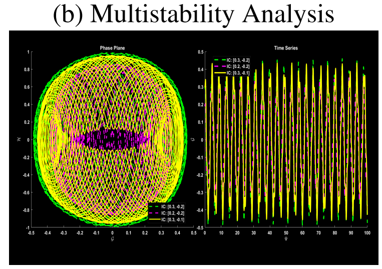

(d) Multistability Analysis

FIGURE 14. Identification of multi-stability in the perturbed system (4. 27), with parameter values $\gamma_1 = -2$, $\gamma_2 = 0.5$, and different values of κ_0, and ω.

4.7. **Power spectrum.** The power spectrum of the system reveals the energy present across the frequencies mapping of $\mathcal{G}(t)$ and $\mathcal{H}(t)$ into the frequency domain. The spectrum displays the main frequencies present and has widened bars, which is characteristic of complex and non-periodic oscillations. There is an absence of a sharply defined peak, suggesting non-linear oscillations and likely chaotic activity in the system.

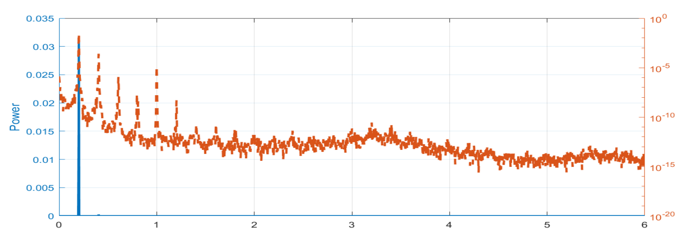

FIGURE 15. Power spectrum graph to the Eq. (4. 27) by utilizing the proper values of parameters

4.8. **Fractal Dimension.** Fig. (16) illustrates the fractal dimension (FD) analysis, which is employed to evaluate the geometric complexity of the attractors and the manner in which the trajectories populate the phase space. In this mapping, the coordinate along the x-axis, $log(r)$, shows the logarithm of the length scale, which for attractors has inverted length in this case, whereas the coordinate along the y-axis, $log(C(r))$, shows the logarithm of the number of boxes needed to describe the attractor given a box of dimension. A linear relation between the above quantities on an entire scaling region gives support for the existence of a scale invariance, which becomes the character of having a fractal dimension because of the non-integer slope found for the latter relation. For the parameters $\kappa_0 = 2.5$ and $\omega = 2\pi$, the fractal dimensions related to the ICs $(0.55, 0.01, 5.1)$ and $(0.05, 0.01, 5.1)$ are calculated and verified with quasi-periodic dynamics. The fractal dimensions calculated here evidence a coverage of a very small part of phase space and prove the trajectory is more complex than a periodic orbit, and on the other hand there is not an irregular filling.

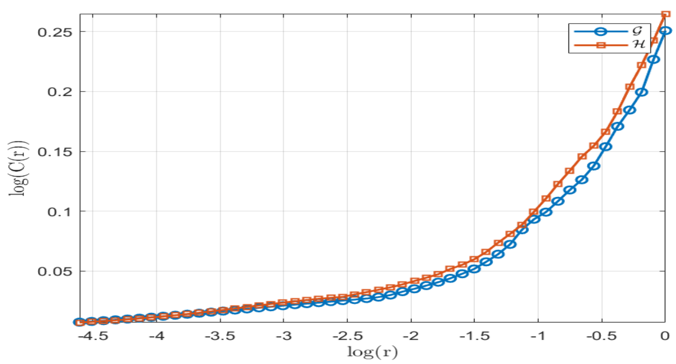

FIGURE 16. Fractal dimension plot to the Eq. (4. 27) by utilizing the proper values of parameters

4.9. **Return Map and Recurrence Plots.** Return maps and recurrence plots are among the most effective techniques for analyzing nonlinear dynamical behavior. A return map is generated by relating each state variable to its successive value, thereby providing a graphical representation of the system evolution. This approach enables the identification of equilibrium states, periodic orbits, quasi-periodic responses, and chaotic attractors through the distribution of the mapped points. Periodic motion typically appears as a finite set of regular points, whereas quasi-periodic and chaotic states produce increasingly complex point distributions. In contrast, a recurrence plot illustrates the instances at which the system trajectory revisits neighborhoods of previously occupied states in the phase space. When employed together, these techniques offer complementary qualitative and quantitative information, enabling a deeper understanding of the geometric structure, evolution, and complexity of the underlying dynamical behavior.

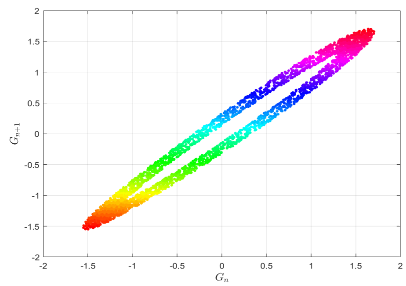

(a) Multistability Analysis

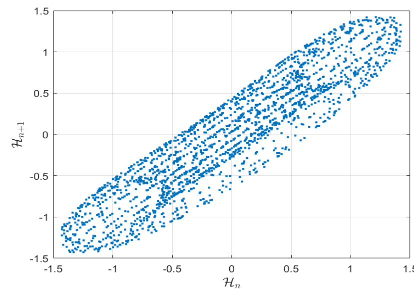

(b) Multistability Analysis

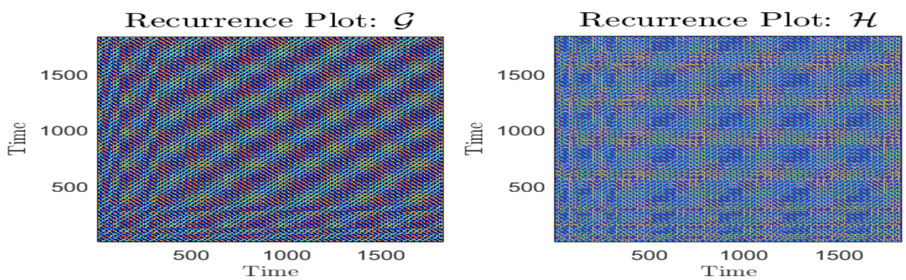

(c) Recurrence plot

FIGURE 17. Recurrence graph to the Eq. (4. 27) by utilizing the proper values of parameters along $\mathcal{G}$ and $\mathcal{H}$.

4.10. **Bifurcation Diagram.** A bifurcation diagram is a fundamental tool in nonlinear dynamics for illustrating how the qualitative behavior of a system evolves as a control parameter is varied. It provides a graphical representation of transitions between different dynamical states, such as periodic, quasi-periodic, and chaotic motions. In the present study, the bifurcation characteristics of the vc-gKP equation are investigated by varying the control parameter κ_0 and recording the corresponding values of the state variable $\mathcal{G}$. This analysis reveals the changes in the stability and multiplicity of the system responses as the external forcing amplitude is modified. When parameters such as $\gamma_0 = 2$,$\gamma_1 = 0.5$, $\kappa_0 = 2.2$, and $\omega = 2\pi$ are used, the system shows different dynamic patterns. The graph demonstrates the way the system changes when the control parameter κ_0 increases from 0.4 to 1.3. When κ_0 is modest (between 0.4 and 1.1), the system shows stable periodic oscillations. The trajectories stay on symmetric branches around the horizontal axis. As κ_0 approaches 1.3, a distinct bifurcation appears, signifying the shift from steady periodic motion to complex kinetics. When $\kappa_0 \geq 1.1$, the system reaches a chaotic state where the trajectories are very irregular and spread out, showing that the system is sensitive to its ICs. For values of $1.1 \leq \kappa_0 \leq 1.3$, the oscillations expand wider, and the system shows patterns of order and disorder that change from one to the other, with periodic windows appearing and disappearing in chaotic areas. The continuous change between order and disorder shows how very sensitive the underlying dynamical model is to the system.

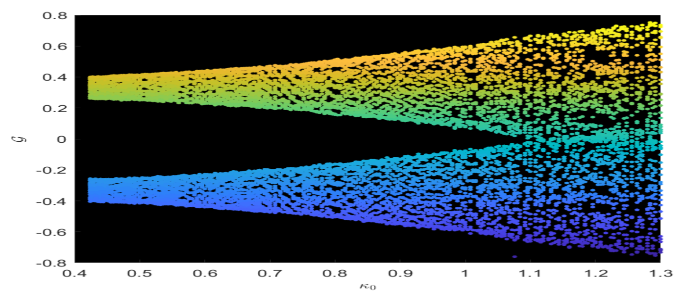

FIGURE 18. Analysis of chaotic phenomena in the dynamical system (4. 27) through bifurcation diagram.

4.11. **Sensitivity analysis.** Sensitivity analysis serves as an important technique for assessing the effect of variations in the input parameters on the system output. This method presents an extensive description regarding the way changes in physical parameters or ICs impact the overall dynamics of the system. The investigation of the current system demonstrates that even little modifications in the ICs lead to significant modifications inside the system. We use the Runge-Kutta method to explore these impacts by numerically solving Eq. (2. 9). The corresponding perturbed dynamical system is formulated as:

$$\begin{cases} \frac{d\mathcal{G}}{d\Psi} = \mathcal{H}, \\ \frac{d\mathcal{H}}{d\Psi} = \gamma_0\mathcal{G} - \gamma_1\mathcal{G}^2 + \kappa_0\cos(\mathcal{M}). \end{cases} \tag{4. 28}$$

To assess the sensitivity of the proposed system, three distinct sets of ICs are analyzed. The trajectories were color-coded as follows: green for $(\mathcal{G}, \mathcal{H}) = (0.15, 0)$, magenta for $(\mathcal{G}, \mathcal{H}) = (0.30, 0)$, and cyan for $(\mathcal{G}, \mathcal{H}) = (0.45, 0)$. In Fig. 19(a), the comparison between the green and magenta curves illustrates the dynamical responses corresponding to $(0.15, 0)$ and $(0.30, 0)$, respectively. Fig. 19(b) presents the trajectories for $(0.15, 0)$ and $(0.45, 0)$, while Fig. 19(c) depicts the solutions for $(0.30, 0)$ and $(0.45, 0)$. Finally, Fig. 19(d) consolidates all three cases, providing a direct comparison among the trajectories generated by $(0.15, 0)$, $(0.30, 0)$, and $(0.45, 0)$. Overall, the analysis confirms that the proposed system is extremely sensitive to ICs. Even very small variations in $(\mathcal{G}, \mathcal{H})$ lead to noticeably different long-term trajectories, ranging from changes in oscillatory amplitude to complete divergence in motion as shown in Fig.19(a-d). Such sensitivity is a defining characteristic of nonlinear dynamical systems and serves as a strong indicator of the model?s potential for complex and chaotic behavior.

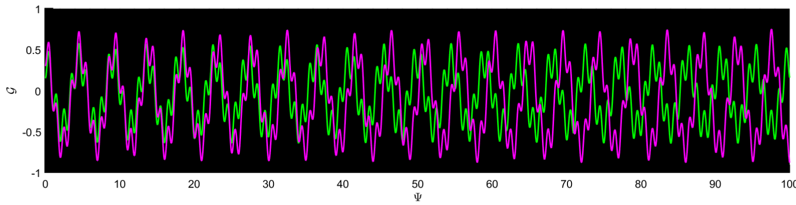

(a) Sensitivity analyzed for $(\mathcal{G}, \mathcal{H}) = (0.15, 0)$

in green and $(\mathcal{G}, \mathcal{H}) = (0.30, 0)$ in magenta.

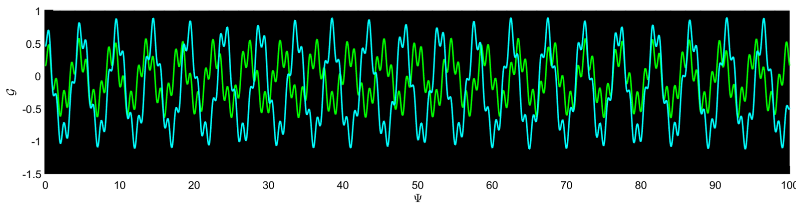

(b) Sensitivity is examined for $(\mathcal{G}, \mathcal{H}) = (0.15, 0)$

in green and $(\mathcal{G}, \mathcal{H}) = (0.45, 0)$ in cyan.

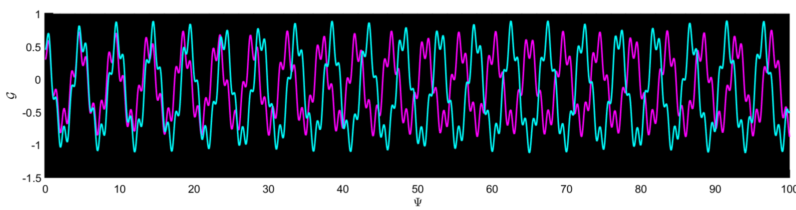

(c) Sensitivity is evaluated for $(\mathcal{G}, \mathcal{H}) = (0.30, 0)$

in magenta and $(\mathcal{G}, \mathcal{H}) = (0.45, 0)$ in cyan.

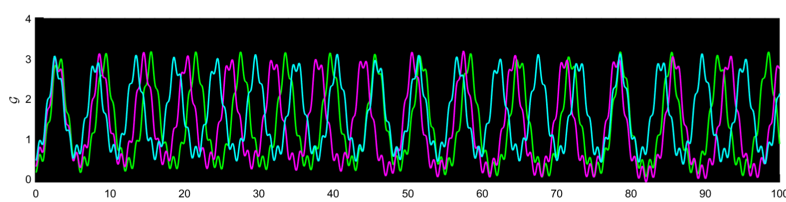

(d) Sensitivity is tested simultaneously for three different sets of initial values: $(\mathcal{G}, \mathcal{H}) = (0.15, 0)$ in green, $(\mathcal{G}, \mathcal{H}) = (0.30, 0)$ in magenta, and $(\mathcal{G}, \mathcal{H}) = (0.45, 0)$ in cyan.

FIGURE 19. Sensitivity analysis on different ICs for the system (4. 28).

5. COMPARATIVE ANALYSIS WITH EXISTING STUDIES

This section presents the comparison of the present work with previous studies conducted on the KP equation in the section below. Most previous work was concerned with obtaining specific analytical and exact solutions; however, the research in this paper focuses on deriving exact wave solutions alongside the overall dynamical behavior. Table (5) summarizes the key differences and highlights the novel contributions of the proposed approach.

TABLE 5. Comparative evaluation of analytical and dynamical tools reported in the literature

Ref.	MKM	BDs	SA	MS	PMs	CB	TS	LEs	RM	RP	FD	PS
[32]	×	×	×	×	×	×	×	×	×	×	×	×
[33]	×	×	×	×	×	×	×	×	×	×	×	×
[34]	×	×	×	×	×	×	×	×	×	×	×	×
[35]	×	×	×	×	×	×	×	×	×	×	×	×
[36]	×	×	×	×	×	×	×	×	×	×	×	×
Our study	✓	✓	✓	✓	✓	✓	✓	✓	✓	✓	✓	✓

6. CONCLUSION

In this study, the $(4+1)$-dimensional vc-gKP equation equation was investigated through a combination of analytical and qualitative approaches, providing a comprehensive understanding of its nonlinear dynamics. The MKM method used to build up an apex multitude of the wave structures, such as rational, trigonometric, and hyperbolic functions, bright-dark soliton and kink-type profiles. These have the added benefit of not only providing improved rigor to the range of admissible wave forms to the vc-gKP equation, but they also provide a strict set of benchmarks to later analytical and numerical efforts. The vc-gKP equation was rewritten to be an autonomous planar dynamical system to obtain better understanding of the system dynamical behavior through Galilean transformation. The results in terms of the bifurcation analysis and phase portrait showed that various forms of equations of equilibrium such as centers, saddles, and cusps exist with varying conditions of parameters. These were also confirmed by the Hamiltonian formulation which showed that the structures observed in phase space were stable and coherent. The reduced system also had abundant nonlinear behaviors, such as periodic, quasi-periodic and chaotic behaviors, when a periodically applied external forcing term was added. Systematic examination of these transitions in terms of phase portraits, bifurcation diagrams, Poincaré maps, Lyapunov exponents and time-series analysis data all indicated that these transitions are highly sensitive to the amplitude, frequency and ICs of forcing. The research also used sophisticated diagnostic tools in order to measure the dynamism of the nonlinear dynamics. The analysis of power spectrum has shown how discrete frequency peaks are shifted to broadband spectra which are evidence of chaotic motion. The use of fractal dimension calculation gave a quantitative analysis of the geometrical complexity of the chaotic attractors to show that they are not integer dimensional. The nonlinear switches between the regular and chaotic behavior were shown with the help of return maps, and complex temporal structures were depicted with the help of recurrence plots which indicated the deterministic chaos and multistability of the system. The sensitivity analysis affirmed that even minor changes in the ICs will result in large differences in the trajectories of the system, which characterizes the nature of chaos in the systems. Generally, the solutions reveal that, they are able to visualize a highly complicated interaction between soliton solutions which are integrable and complex chaotic dynamics in the (4+1)-dimensional vc-gKP model. These exact analytic solutions coupled with qualitative dynamical analysis give a strong platform towards the study of the nonlinear development of high dimensional wave systems. It has far-reaching consequences in any nonlinear field of science, such as fluid mechanics, nonlinear optics, plasma physics, oceanography, and other applications where wave propagation, multi-stability and chaos are issues of great importance. Building upon the present analytical and dynamical framework, future research will focus on investigating more general higher-dimensional variable-coefficient nonlinear evolution equations with additional physical effects, such as damping, variable external forcing, and nonlocal interactions, to further explore their influence on soliton dynamics and nonlinear stability.

Author Contributions Statement

Muhammad Iqbal: Conceptualization, methodology, mathematical analysis, software, visualization, validation, formal analysis, investigation, and writing original draft. Muhammad Aziz ur Rehman: Supervision, conceptualization, methodology, validation, critical review, and editing of the manuscript. Zaheer Hussain Shah: Supervision, formal analysis, validation, interpretation of results, and critical review and editing. All authors contributed to the discussion of the results, reviewed the manuscript critically, and approved the final version for publication.

Declarations

Conflict of Interest. The authors declare that they have no conflict of interest regarding the publication of this research.
Funding. No funding was received for or associated with this research.
Acknowledgments. The authors gratefully acknowledge the University of Management and Technology (UMT), Lahore, Pakistan, for providing the academic environment and facilities that supported this research.
Data Availability. All data used in this study are available within the manuscript.

References

[1] H. Ahmad, M. N. Alam, and M. Omri, *New computational results for a prototype of an excitable system*, Results in Physics **28** (2021) 104666.

[2] A. Ali, J. Ahmad, S. Javed, and S. U. Rehman, *Analysis of chaotic structures, bifurcation and soliton solutions to fractional Boussinesq model*, Physica Scripta **98**, No. 7 (2023) 075217.

[3] K. K. Ali, S. Tarla, A. Yusuf, and R. Yilmazer, *Closed form wave profiles of the coupled-Higgs equation via the ϕ_6-model expansion method*, International Journal of Modern Physics B **37**, No. 7 (2023) 2350070.

[4] K. K. Ali, A. Yusuf, and W. X. Ma, *Dynamical rational solutions and their interaction phenomena for an extended nonlinear equation*, Communications in Theoretical Physics **75**, No. 3 (2023) 035001.

[5] S. Bibi, S. T. Mohyud-Din, U. Khan, and N. Ahmed, *Khater method for nonlinear Sharma-Tasso-Olver (STO) equation of fractional order*, Results in Physics **7** (2017) 4440–4450.

[6] A. Biswas, M. Mirzazadeh, M. Eslami, Q. Zhou, A. Bhrawy, and M. Belic, *Optical solitons in nano-fibers with spatio-temporal dispersion by trial solution method*, Optik **127**, No. 18 (2016) 7250–7257.

[7] S. Dehraj, M. H. Baig, S. Munwer, and D. U. Sarwe, *Novel solitary wave solutions for nonlinear fractional BBM and (2+1)-dimensional extended KP equations via* $e^{-\psi(\zeta)}$ *expansion approach*, Punjab University Journal of Mathematics **57**, No. 11 (2025) 1190.

[8] A. L. Fabian, R. Kohl, and A. Biswas, *Perturbation of topological solitons due to sine-Gordon equation and its type*, Communications in Nonlinear Science and Numerical Simulation **14**, No. 4 (2009) 1227–1244.

[9] E. Fermi, J. R. Pasta, and S. M. Ulam, *Studies of nonlinear problems*, Los Alamos Scientific Laboratory Report LA-1940 (1955).

[10] Y. Gu, X. Zhang, L. Peng, Z. Huang, and Y. Lai, *Lump and new interaction solutions of the (3+1)-dimensional generalized shallow water-like equation along with chaotic analysis*, Alexandria Engineering Journal **126** (2025) 160–169.

[11] J. H. He and G. C. Wu, *Austin, The variational iteration method which should be followed*, Nonlinear Science Letters A **1** (2010) 1–30.

[12] R. L. Horne, *A (very) brief introduction to soliton theory in a class of nonlinear PDEs*, Mathematical Sciences Proceedings **3** (2002).

[13] K. Hosseini, M. Mirzazadeh, D. Baleanu, S. Salahshour, and L. Akinyemi, *Optical solitons of a high-order nonlinear Schrödinger equation involving nonlinear dispersions and Kerr effect*, Optical and Quantum Electronics **54**, No. 3 (2022) 177.

[14] M. Irshad, M. Hussan, M. Shan, Z. Ali, U. Fatima, and I. Jahangir, *Exploring Lie point symmetries and exact solutions for (1+1)-dimensional modified Thomas and (1+2)-dimensional Chaffee-Infante equations*, Punjab Univ. j. Math. **56**, No. 9 (2024) 567–591.

[15] M. Jamil, R. A. Khan, and K. Shah, *Exact analytical solutions of linear dissipative wave equations via Laplace transform method*, Punjab Univ. j. Math. **53**, No. 6 (2021) 425–434.

[16] A. Jhangeer, H. Almusawa, and Z. Hussain, *Bifurcation study and pattern formation analysis of a nonlinear dynamical system for chaotic behavior in traveling wave solution*, Results in Physics **37** (2022) 105492.

[17] Y. S. Kivshar, *Stable vector solitons composed of bright and dark pulses*, Optics Letters **17**, No. 19 (1992) 1322–1324.

[18] D. J. Korteweg and G. de Vries, *XLI. On the change of form of long waves advancing in a rectangular canal, and on a new type of long stationary waves*, The London, Edinburgh, and Dublin Philosophical Magazine and Journal of Science **39**, No. 240 (1895) 422–443.

[19] P. D. Lax, *Integrals of nonlinear equations of evolution and solitary waves*, Communications on Pure and Applied Mathematics **21**, No. 4 (1968) 467–490.

[20] M. Li, L. Wang, and F. H. Qi, *Nonlinear dynamics of a generalized higher-order nonlinear Schrödinger equation with a periodic external perturbation*, Nonlinear Dynamics **86** (2016) 535–541.

[21] D. Lu, B. Hong, and L. Tian, *Bäcklund transformation and n-soliton-like solutions to the combined KdV-Burgers equation with variable coefficients*, International Journal of Nonlinear Science **2**, No. 1 (2006) 3–10.

[22] Y. L. Ma and B. Q. Li, *Bifurcation solitons and breathers for the nonlocal Boussinesq equations*, Applied Mathematics Letters **124** (2022) 107677.

[23] F. Marin, *Solitons: Historical and physical introduction*, in *Solitons*, 237–255, Springer, New York (2022).

[24] F. Meng, S. Shi, B. Zhang, M. Bai, and N. Lin, *Analysis for global characteristics of Lyapunov exponents in vehicle plane motion system*, Scientific Reports **12**, No. 1 (2022) 9300.

[25] N. C. T. Mezamo, V. B. Nana, F. W. Tchuimmo, and L. Nana, *Stabilization of traveling waves on dissipative system near subcritical bifurcation through a combination of global and local feedback*, The European Physical Journal Plus **137** (2022) 1139.

[26] N. Mhadhbi, S. Gana, and M. F. Alsaeedi, *Exact solutions for nonlinear partial differential equations via a fusion of classical methods and innovative approaches*, Scientific Reports **14**, No. 1 (2024) 6443.

[27] B. Mohan and S. Kumar, *Painlevé analysis, restricted bright-dark N-solitons, and N-rogue waves of a (4+1)-dimensional variable-coefficient generalized KP equation in nonlinear sciences*, Nonlinear Dynamics **113**, No. 10 (2025) 11893–11906.

[28] M. Modanli, M. A. S. Murad, and S. T. Abdulazeez, *A new computational method-based integral transform for solving time-fractional equation arises in electromagnetic waves*, Zeitschrift für angewandte Mathematik und Physik **74**, No. 5 (2023) 186.

[29] N. Raza, A. Jhangeer, S. Arshed, A. R. Butt, and Y. M. Chu, *Dynamical analysis and phase portraits of two-mode waves in different media*, Results in Physics **19** (2020) 103650.

[30] A. B. Shabat and V. E. Zakharov, *Exact theory of two-dimensional self-focusing and one-dimensional self-modulation of waves in nonlinear media*, Soviet Physics JETP **34**, No. 1 (1972) 62–69.

[31] A. Shahhosseini, M. H. Tien, and K. D'Souza, *Poincaré maps: A modern systematic approach toward obtaining effective sections*, Nonlinear Dynamics **111**, No. 1 (2023) 529–548.

[32] J. Singh, D. Kumar, Z. Hammouch, and A. Atangana, *A fractional epidemiological model for computer viruses pertaining to a new fractional derivative*, Applied Mathematics and Computation **316** (2018) 504–515.

[33] L. Tang, A. Biswas, Y. Yildirim, and A. Asiri, *Bifurcation analysis and chaotic behavior of the concatenation model with power-law nonlinearity*, Contemporary Mathematics **4** (2023) 1014–1025.

[34] S. Tarla, K. K. Ali, R. Yilmazer, and A. Yusuf, *Investigation of the dynamical behavior of the Hirota-Maccari system in single-mode fibers*, Optical and Quantum Electronics **54**, No. 10 (2022) 613.

[35] M. S. Ullah, *Interaction solution to the (3+1)-D negative-order KdV first structure*, Partial Differential Equations in Applied Mathematics **8** (2023) 100566.

[36] M. S. Ullah, M. Mostafa, M. Z. Ali, H. O. Roshid, and M. Akter, *Soliton solutions for the Zoomeron model applying three analytical techniques*, PLoS ONE **18**, No. 7 (2023) e0283594.

[37] M. Wadati, *Introduction to solitons*, Pramana **57**, No. 5 (2001) 841–847.

[38] K. Wang, *Exact traveling wave solutions for the local fractional Kadomtsev-Petviashvili-Benjamin-Bona-Mahony model by variational perspective*, Fractals **30**, No. 6 (2022) 2250101.

[39] K. Wang, *Exact traveling wave solution for the local fractional Camassa-Holm-Kadomtsev-Petviashvili equation*, Alexandria Engineering Journal **63** (2023) 371–376.

[40] N. J. Zabusky and M. D. Kruskal, *Interaction of "solitons" in a collisionless plasma and the recurrence of initial states*, Physical Review Letters **15**, No. 6 (1965) 240–243.